An Interaction Landscape of Ubiquitin Signaling

Zhang, X.F.; Smits, A.H.; Tilburg, G.B.A. van; Jansen, P.W.T.C.; Makowski, M.M.; Ovaa, H.; Vermeulen, M.

Resource

Molecular Cell

An Interaction Landscape of Ubiquitin Signaling

Graphical Abstract

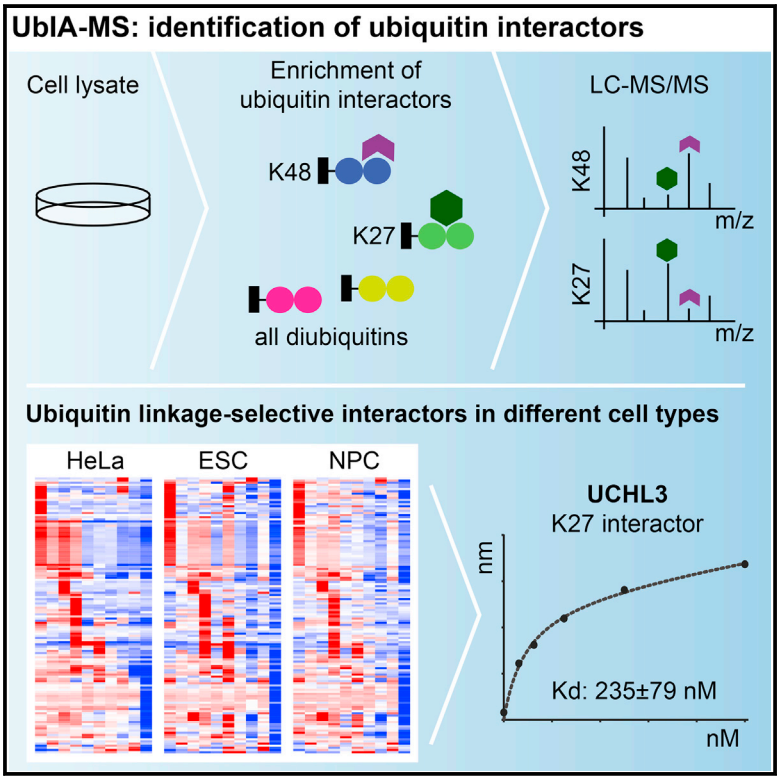

Highlights

- UbIA-MS enables proteome-wide profiling of ubiquitin signaling interactors
- Resource of ubiquitin linkage-selective interactors in multiple cell types
- The inter-UIM region determines selective binding to K48 and K63 ubiquitin linkages
- Deubiquitinase UCHL3 selectively binds to and regulates K27 ubiquitin linkages

Authors

Xiaofei Zhang, Arne H. Smits, Gabrielle B.A. van Tilburg, Pascal W.T.C. Jansen, Matthew M. Makowski, Huib Ovaa, Michiel Vermeulen

Correspondence

x.zhang@science.ru.nl (X.Z.), h.ovaa@lumc.nl (H.O.), michiel.vermeulen@science.ru.nl (M.V.)

In Brief

Zhang et al. report UbIA-MS, a mass-spectrometry-based proteomics workflow to comprehensively study interactions between proteins and ubiquitin linkages, based on in vitro pull-downs with chemically synthesized diubiquitins. Their work reports a rich resource of linkage-selective as well as general ubiquitin interactors in different cell types and upon cellular perturbation.

Data Resources

PXD004185

Zhang et al., 2017, Molecular Cell *65*, 941–955
March 2, 2017
http://dx.doi.org/10.1016/j.molcel.2017.01.004

Molecular Cell
Resource

An Interaction Landscape of Ubiquitin Signaling

Xiaofei Zhang,[1,4,5,*] Arne H. Smits,[1,4,6,7] Gabrielle B.A. van Tilburg,[2,3,4] Pascal W.T.C. Jansen,[1] Matthew M. Makowski,[1] Huib Ovaa,[2,3,*] and Michiel Vermeulen[1,8,*]
[1]Department of Molecular Biology, Faculty of Science, Radboud Institute for Molecular Life Sciences, Radboud University Nijmegen, Nijmegen 6525, the Netherlands
[2]Division of Cell Biology II, Netherlands Cancer Institute, Plesmanlaan 121, Amsterdam 1066CX, the Netherlands
[3]Department of Chemical Immunology, Leiden University Medical Center, Albinusdreef 2, Leiden 2333ZA, the Netherlands
[4]Co-first author
[5]Present address: Key Laboratory of Regenerative Biology of the Chinese Academy of Sciences and Guangdong Provincial Key Laboratory of Stem Cells and Regenerative Medicine, South China Institute for Stem Cell Biology and Regenerative Medicine, Guangzhou Institutes of Biomedicine and Health, Chinese Academy of Sciences, Guangzhou 510530, China
[6]Present address: Genome Biology Unit, European Molecular Biology Laboratory, 69117 Heidelberg, Germany
[7]Present address: Cellzome, Molecular Discovery Research, GlaxoSmithKline, 69117 Heidelberg, Germany
[8]Lead Contact
*Correspondence: x.zhang@science.ru.nl (X.Z.), h.ovaa@lumc.nl (H.O.), michiel.vermeulen@science.ru.nl (M.V.)
http://dx.doi.org/10.1016/j.molcel.2017.01.004

SUMMARY

Intracellular signaling via the covalent attachment of different ubiquitin linkages to protein substrates is fundamental to many cellular processes. Although linkage-selective ubiquitin interactors have been studied on a case-by-case basis, proteome-wide analyses have not been conducted yet. Here, we present ubiquitin interactor affinity enrichment-mass spectrometry (UbIA-MS), a quantitative interaction proteomics method that makes use of chemically synthesized diubiquitin to enrich and identify ubiquitin linkage interactors from crude cell lysates. UbIA-MS reveals linkage-selective diubiquitin interactions in multiple cell types. For example, we identify TAB2 and TAB3 as novel K6 diubiquitin interactors and characterize UCHL3 as a K27-linkage selective interactor that regulates K27 polyubiquitin chain formation in cells. Additionally, we show a class of monoubiquitin and K6 diubiquitin interactors whose binding is induced by DNA damage. We expect that our proteome-wide diubiquitin interaction landscape and established workflows will have broad applications in the ongoing efforts to decipher the complex language of ubiquitin signaling.

INTRODUCTION

Ubiquitination entails the covalent but reversible attachment of the 76-amino-acid protein ubiquitin to, in most cases, a lysine residue on protein substrates. Three enzymes, namely E1-activating enzyme, E2-conjugating enzyme, and E3 ligase, are required to catalyze the conjugation of ubiquitin to target proteins. Another class of enzymes called deubiquitinases (DUBs) can remove ubiquitin molecules from proteins. Ubiquitination can be classified as monoubiquitination, multi-monoubiquitination, and polyubiquitination according to the number and topology of ubiquitin molecules that are conjugated to the substrate. Ubiquitination alters the function of protein substrates and ubiquitin signaling therefore plays an important role in essentially all cellular processes. For example, monoubiquitination alters protein activity and subcellular localization, K48 polyubiquitination targets substrates for proteasomal degradation, and K63 or linear polyubiquitin (polyUb) chains serve as protein-protein interaction platforms to mediate signal transduction (Komander and Rape, 2012).

The complexity of ubiquitin signaling is augmented by polyUb chains with distinct topologies. Eight homotypic polyUb linkages are known to exist and are linked via the C terminus of donor ubiquitin and any of the seven lysine residues (Lys6, Lys11, Lys27, Lys33, Lys48, and Lys63) or the amino terminal methionine residue (Met1) of the acceptor ubiquitin. Recent studies also revealed the in vivo existence of branched and mixed polyUb chains (Peng et al., 2003; Emmerich et al., 2013; Meyer and Rape, 2014). Another layer of complexity is added by post-translational modifications (PTMs) of ubiquitin, including acetylation and phosphorylation (Herhaus and Dikic, 2015). All of these structurally unique polyUb chains and ubiquitin PTMs make up a "ubiquitin code" that determines the function and fate of protein substrates.

How do cells decode this ubiquitin code into proper cellular responses? Recent studies have indicated that members of a protein family, ubiquitin-binding proteins (UBPs), mediate the recognition of ubiquitinated substrates. UBPs contain at least one of 20 ubiquitin-binding domains (UBDs) functioning as a signal adaptor to transmit the signal from ubiquitinated substrates to downstream effectors (Husnjak and Dikic, 2012). Since many UBDs recognize the same hydrophobic binding patch on ubiquitin (Ile44-Leu8-Val70), the nature of UBP selective recognition of different ubiquitin linkages remains elusive. Nevertheless, accumulating evidence suggests that many UBDs selectively bind to particular ubiquitin linkages (Husnjak and Dikic, 2012; Komander and Rape, 2012). Linkage-selective interactions are achieved either by a single UBD that binds to a certain ubiquitin linkage with high affinity or by multiple UBDs that

cooperatively bind with high avidity to a specific ubiquitin linkage. For different ubiquitin linkages, the selective recognition by UBDs depends on the spatial distribution of ubiquitin moieties (Husnjak and Dikic, 2012). In addition, a linker region between ubiquitin moieties can determine ubiquitin linkage-selective interactions, as exemplified by the selective interaction between NEMO and Met1 linkages (Rahighi et al., 2009). Mutagenesis studies have revealed that the selective ubiquitin binding activity of UBPs regulates important cellular functions, as illustrated by several UBDs that are involved in regulating nuclear factor κB (NF-κB) signaling (Husnjak and Dikic, 2012). More importantly, mutations in UBDs of NEMO and ABIN1 have been found in patients with inflammatory diseases (Cohen, 2014). These examples emphasize that studying UBP-ubiquitin interactions on a proteome-wide scale would be of great value to decipher the functions of ubiquitin signaling in health and disease.

The development of specific enrichment tools to detect and quantify ubiquitinated peptides by mass spectrometry (MS) has significantly increased our knowledge about the ubiquitylome (Xu et al., 2010). This method has also been used to decipher the dynamics of the ubiquitylome upon certain stimuli such as induction of DNA damage (Elia et al., 2015). However, proteome-wide interaction analyses of ubiquitin signaling have not been reported, mainly due to the lack of proper tools. Recent advances in chemical biology have enabled in vitro synthesis of all homotypic, isopeptide-linked diubiquitins (diUbs) (Kumar et al., 2010; El Oualid et al., 2010), and advances in quantitative proteomics have enabled the comprehensive identification of protein-protein interactions (Smits and Vermeulen, 2016). Here, we present ubiquitin interactor affinity enrichment-mass spectrometry (UbIA-MS) to identify interactors of all ubiquitin linkages in a variety of cell types. We used non-hydrolyzable diUbs, which can prevent premature chain cleavage by DUBs (Eger et al., 2010; Flierman et al., 2016), as affinity enrichment baits in crude mammalian cell lysates followed by liquid chromatography-tandem MS (LC-MS/MS). Our data revealed cell-type- and expression-dependent and independent linkage-selective ubiquitin interactors. Additionally, dynamic K6 diUb interactions were identified upon induction of DNA damage. To exemplify the richness of this dataset, we elaborated on the binding selectivity of the NZF domain of TAB2/3 to K6 ubiquitin linkages. Furthermore, we showed that UCHL3 preferentially binds to K27 diUb and that its catalytic site is important for regulating K27 polyUb chains in cells. Taken together, our work provides both a proteome-wide interaction map for ubiquitin signaling and a robust and unbiased workflow that can be used to investigate how cells decipher ubiquitin signaling when perturbed.

RESULTS

UbIA-MS: Mass-Spectrometry-Based Workflow to Identify Interactors for Ubiquitin Signaling

To establish a workflow to systematically identify proteins interacting with ubiquitin chains, we performed in vitro pull-downs using linear polyUb chains and stable isotope labeling with amino acids in cell culture (SILAC)-labeled whole-cell extracts followed by high-resolution LC-MS/MS (Figure 1A). Initially, we compared in-gel and on-bead digestion for sample preparation (Figures 1B and 1C). As shown in Figures 1B–1D and Table S1, available online, we identified 111 and 53 selective interactors for linear polyUb chains by in-gel and on-bead digestion, respectively. In-gel digestion typically achieves deeper sample coverage compared to on-bead digestion, yet the most pronounced interactors are shared between both experiments (Figure 1D; Table S1). Therefore, we decided to use the on-bead digestion protocol for further experiments as this workflow reduces the number of samples to be measured by a factor of eight compared to in-gel digestion.

Among the 46 interactors identified by both workflows, 6 are known to bind to linear linkages, including the linear ubiquitin assembly complex (SHARPIN-RNF31-RBCK1), FAM105B, TNIP1, and IKBKG (Iwai et al., 2014). All these proteins are involved in regulating NF-κB signaling, which is in agreement with the known pivotal role of linear ubiquitination in regulating NF-κB signaling (Iwai et al., 2014). It should be noted that not all identified interactors necessarily bind to linear polyUb chains through direct interactions. For example, the interaction between IKBKB or CHUK and linear polyUb chains is most likely indirect, since no obvious interactions between these proteins were observed when purified proteins were incubated with linear polyUb chains (data not shown). Taken together, these results indicate that UbIA-MS represents an efficient workflow to systematically identify interactors for ubiquitin chains.

Identification of Linkage-Selective diUb Interactors in HeLa Cells

To obtain a global interactome of all ubiquitin linkages, we adopted a chemical synthesis method to produce all eight diUbs in a non-hydrolyzable form, containing an N-terminal biotin moiety and a small polyethylene glycol (PEG) spacer at the distal end (Figures S1A–S1C) (Eger et al., 2010; Ekkebus et al., 2013). The formed triazole linkage, which is resistant to cleavage by endogenous DUBs, has been shown to be a good mimic of the isopeptide bond as present in native glycine-ε-lysine diUb (Weikart et al., 2012; Flierman et al., 2016). To verify the functionality of the triazole linkage in non-hydrolyzable diUb, we determined the binding constant between the RAD23A UBA2 domain and K48 diUb (closed conformation) as well as the binding constant between the TAB2 NZF domain and K63 diUb (open conformation) (Husnjak and Dikic, 2012). In concordance with previous reports, the RAD23A UBA2 domain and the TAB2 NZF domain selectively interact with native and non-hydrolyzable K48 and K63 diUb, respectively (Figures S2A and S2B). For both domains, we observed a slightly lower binding affinity for native compared to non-hydrolyzable diUb. This is likely due to the different chemistries that were used to biotinylate native and non-hydrolyzable diUbs: non-hydrolyzable diUbs were uniformly biotinylated at the N terminus, whereas native diUbs were biotinylated through an N-hydroxysuccinimide (NHS) reactive moiety at primary amine sites. The biotinylation of native diUbs at random amines and the fact that a small portion of those carry a second biotin moiety could potentially obscure UBP binding to selective ubiquitin recognition patches. Nevertheless, the measured interactions with non-hydrolyzable diUbs analogs provide a good approximation of the interactions with native diUbs.

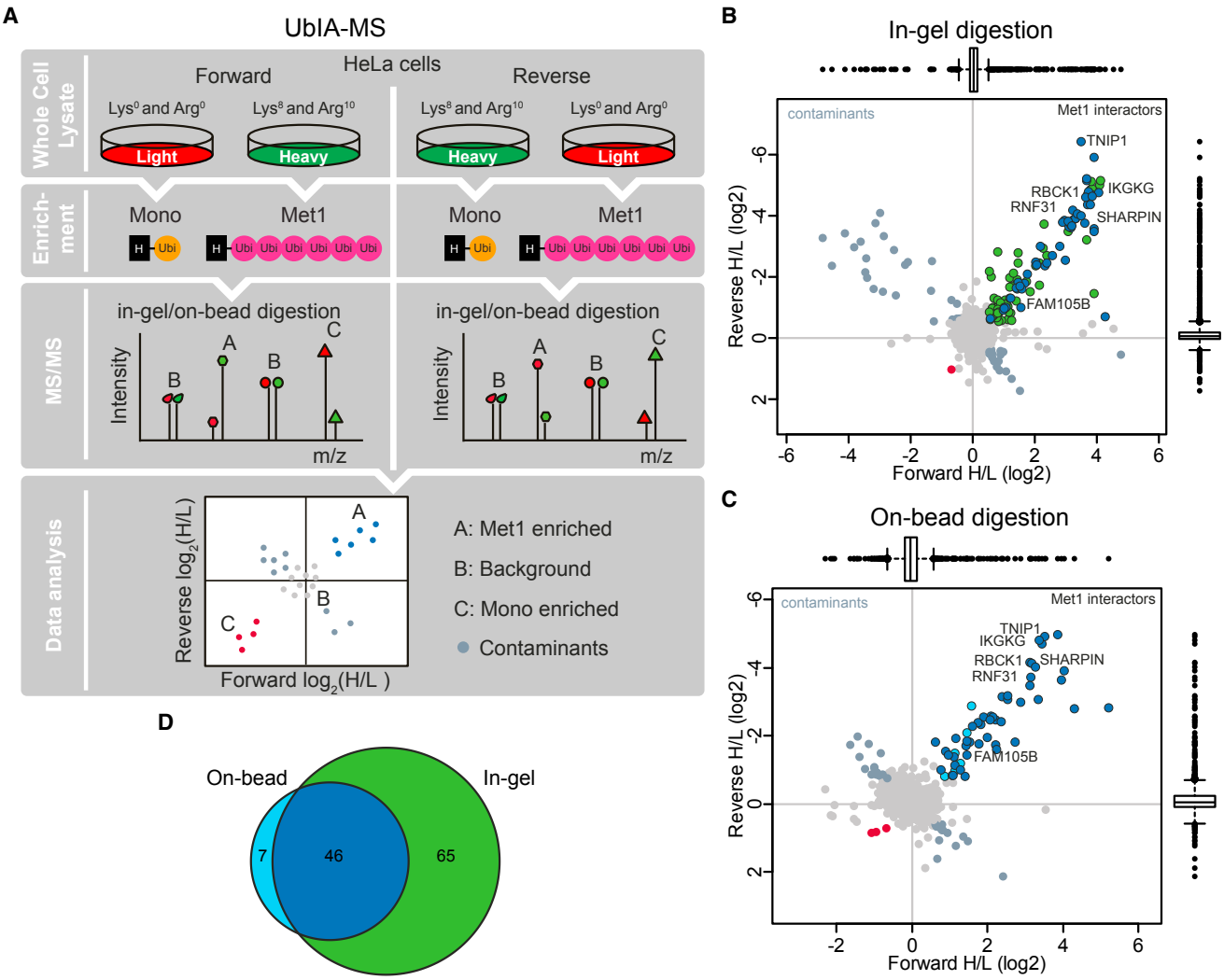

Figure 1. Identification of Linear Ubiquitin Linkage Interactors

(A) Schematic overview of the SILAC-based quantitative UbIA-MS workflow to identify interactors for linear hexa-ubiquitin chains.

(B and C) Scatterplots of the in-gel (B) and on-bead (C) digestion-based linear ubiquitin chains pull-downs in HeLa whole-cell extracts. Blue, significant interactors shared between the in-gel and on-bead digestion based workflow; green, significant linear ubiquitin interactors only found in in-gel digestion (B); cyan, significant linear ubiquitin interactors only found in on-bead digestion (C); gray, background proteins; red, significant monoUb interactors; dark gray, contaminant proteins. The boxplots along the scatterplots are used for robust outlier detection in both the forward SILAC experiment (boxplot on the top) and the reverse SILAC experiment (boxplot on the right).

(D) Venn diagram showing overlap of significant interactors identified using the in-gel and on-bead digestion workflows (color as in B and C).

See also Table S1.

We then performed UbIA-MS using non-hydrolyzable diUb in HeLa whole-cell extracts with label-free quantitative MS, which allows comparing relative protein abundances between multiple pull-downs (Figure 2A) (Spruijt et al., 2013; Smits et al., 2013). Significantly enriched proteins were identified by ANOVA statistics (thresholds were as follows: false discovery rate [FDR] = 0.0001 and S_0 = 1). Correlation-based clustering of the 243 significant interactors revealed proteins with selective binding to a single or multiple diUbs (Figure 2B; Table S1). Correlating the interaction data with previously generated global absolute proteome data for HeLa cells revealed that our interaction screening is not biased toward high-abundant proteins (Figure S2C) (Nagaraj et al., 2011).

In agreement with previous studies, many known linkage-selective UBPs were detected in our screen, such as ZRANB1 (also known as TRABID) for K29 and K33, proteasome components for K48, BRCA1-A complex for K63, and NEMO (IKBKG) for Met1-linked diUb (Cooper et al., 2009; Licchesi et al., 2011; Kristariyanto et al., 2015; Michel et al., 2015). We also validated some of the detected interactions using immunoblotting (Figure 2C, top), which are in excellent agreement with the MS data (Figure 2C, bottom), thus emphasizing the quality of the data.

Gene ontology (GO) term enrichment analysis of the identified interactors highlight the importance of ubiquitin signaling in many cellular processes (Figures 2D and S2D–S2J; Table S1).

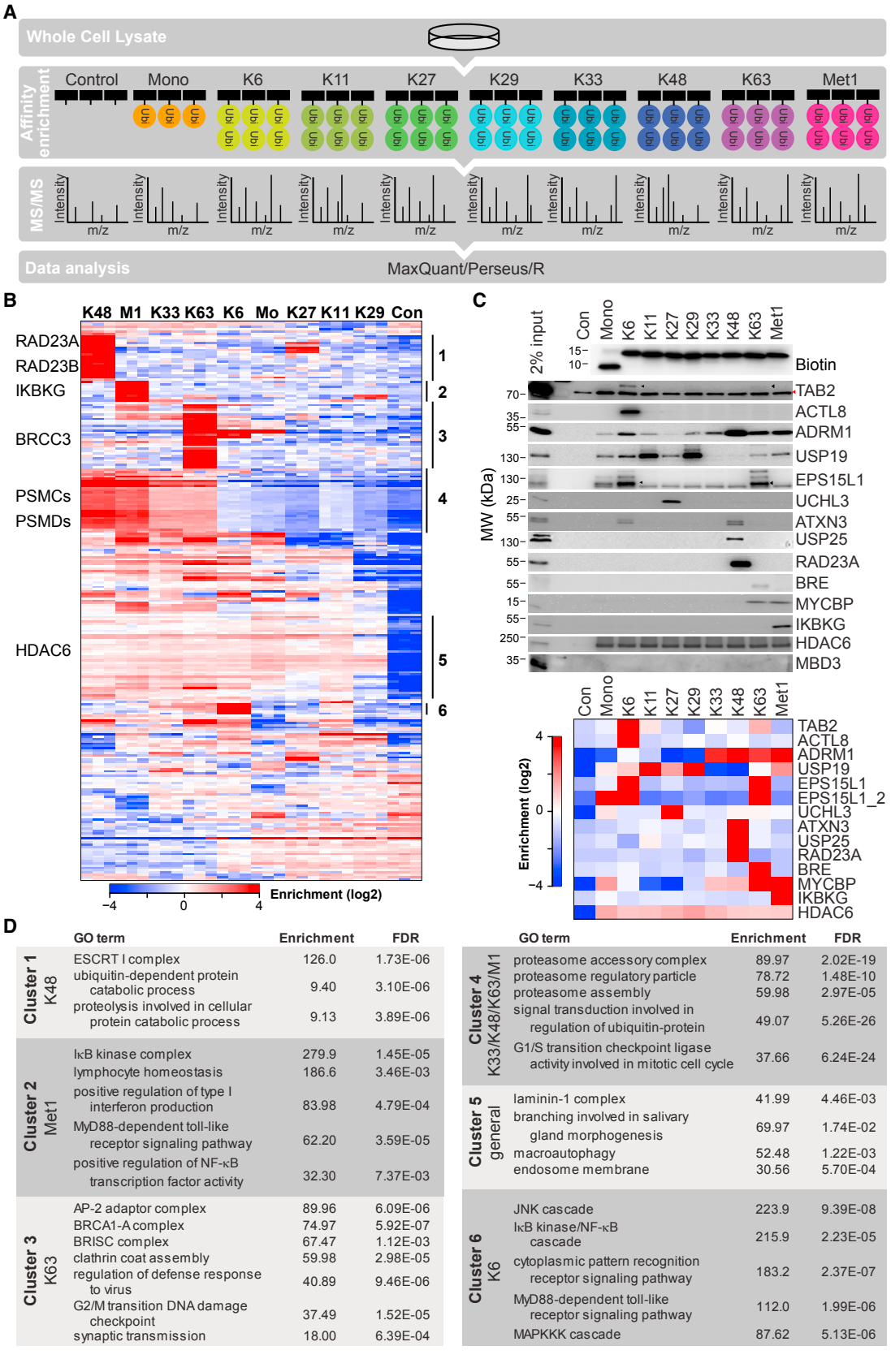

D

	GO term	Enrichment	FDR
Cluster 1 K48	ESCRT I complex	126.0	1.73E-06
	ubiquitin-dependent protein catabolic process	9.40	3.10E-06
	proteolysis involved in cellular protein catabolic process	9.13	3.89E-06
Cluster 2 Met1	IκB kinase complex	279.9	1.45E-05
	lymphocyte homeostasis	186.6	3.46E-03
	positive regulation of type I interferon production	83.98	4.79E-04
	MyD88-dependent toll-like receptor signaling pathway	62.20	3.59E-05
	positive regulation of NF-κB transcription factor activity	32.30	7.37E-03
Cluster 3 K63	AP-2 adaptor complex	89.96	6.09E-06
	BRCA1-A complex	74.97	5.92E-07
	BRISC complex	67.47	1.12E-03
	clathrin coat assembly	59.98	2.98E-05
	regulation of defense response to virus	40.89	9.46E-06
	G2/M transition DNA damage checkpoint	37.49	1.52E-05
	synaptic transmission	18.00	6.39E-04

	GO term	Enrichment	FDR
Cluster 4 K33/K48/K63/M1	proteasome accessory complex	89.97	2.02E-19
	proteasome regulatory particle	78.72	1.48E-10
	proteasome assembly	59.98	2.97E-05
	signal transduction involved in regulation of ubiquitin-protein	49.07	5.26E-26
	G1/S transition checkpoint ligase activity involved in mitotic cell cycle	37.66	6.24E-24
Cluster 5 general	laminin-1 complex	41.99	4.46E-03
	branching involved in salivary gland morphogenesis	69.97	1.74E-02
	macroautophagy	52.48	1.22E-03
	endosome membrane	30.56	5.70E-04
Cluster 6 K6	JNK cascade	223.9	9.39E-08
	IκB kinase/NF-κB cascade	215.9	2.23E-05
	cytoplasmic pattern recognition receptor signaling pathway	183.2	2.37E-07
	MyD88-dependent toll-like receptor signaling pathway	112.0	1.99E-06
	MAPKKK cascade	87.62	5.13E-06

(legend on next page)

Interactors for K6 and Met1 diUbs are enriched for NF-κB signaling, whereas interactors for K63 diUb contain members of AP-2 adaptor complex, which is required for clathrin-mediated endocytosis. In addition, proteasome components interact strongly with K48 and Met1 and, to a lesser extent, with K33 and K63 diUbs. Other diUbs may need to assemble into heterotypic polyUb chains to interact strongly with the proteasome, as was reported for K11-linked polyUb chains, which require heterotypic chain formation with K48 for efficient proteasome interaction (Meyer and Rape, 2014; Grice et al., 2015).

Next, we investigated whether specific UBDs dictate binding preferences for certain diUbs. As shown in Figure S2K, most UBDs have different linkage selectivity in the context of different UBPs, indicating that those UBDs do not preferentially bind to particular linkage(s). Nevertheless, UBPs with tandem ubiquitin-interacting motifs (tUIMs) often exhibit preferential binding to K48 and K63 diUbs (also see Figure 4). In addition, many UBPs with zf-UBP (zinc-finger UBP type) bind similarly to monoubiquitin (monoUb) and all diUbs, which may be explained by the fact that the C terminus of ubiquitin inserts into the binding pocket of zf-UBPs, as exemplified by the interaction between USP5 and monoUb (Reyes-Turcu et al., 2006).

Cell-Type-Dependent and Independent diUb Interactors

Having established UbIA-MS to identify interactors for all diUbs in a proteome-wide and unbiased manner, we investigated whether and to what extent ubiquitin interactions are cell-type specific. To this end, we performed UbIA-MS experiments with lysates from mouse embryonic stem cells (ESCs) and neuronal precursor cells (NPCs) (Figure S2J). As shown in Figures S3A and S3B and Table S1, we identified 381 and 245 significant interactors (thresholds were as follows: FDR = 0.0005, S_0 = 2) in ESCs and NPCs, respectively. Linkage interactions are correlated between ESCs and NPCs, and in particular, K29, K48, K63, and Met1 diUbs interactors show high correlations ($p > 0.7$) (Figure 3A). This suggests that these linkages may have cell-type-independent functions. Hierarchical clustering of the identified 441 significant interactors in NPCs and ESCs revealed that 230 of these (52%) show conserved binding patterns in both cell types (Figures 3B and 3C; Table S1). In addition, we identified 156 and 51 cell-type-specific interactors in ESCs and NPCs, respectively.

To determine whether these dynamic interactions are caused by differential protein expression, we quantified protein copy numbers in ESCs and NPCs using intensity-based absolute quantification (iBAQ) (Figure S3C) (Schwanhäusser et al., 2011). In total, ~8,000 proteins were quantified (Table S1). GO term enrichment analysis of ESC enriched proteins (>10-fold higher than NPC) identified significant overrepresentation of terms such as regulation of chromosome segregation, DNA damage, and mitosis, which may be due to the higher proliferation rate of ESCs compared with NPCs. NPC enriched proteins (>10-fold higher than ESCs) were enriched for neuronal differentiation and synaptic functions, as expected (Figure S3D). The absolute copy numbers of significant interactors span approximately seven orders of magnitude in abundance, indicating that our results are not biased toward highly abundant proteins (Figure S3E). For cell-type-specific interactors, 79 proteins (38%) show correlation between the observed interaction pattern and protein abundance (>2-fold change and $p < 0.05$). One such expression-dependent, cell-type-specific interactor is *Usp38*, which selectively binds to K29 diUb and whose expression is ~7-fold higher in ESCs than in NPCs (Table S1). Of the 131 proteins that do not show correlation between interaction pattern and protein abundance, 23 proteins were not quantified in the iBAQ measurements (Table S1). Expression-independent, cell-type-specific ubiquitin binding may be explained by PTMs or differentially expressed cofactors that may confer linkage-specific ubiquitin binding. Further studies, however, are needed to address this question.

Considering the fact that ubiquitin itself is highly conserved in eukaryotic evolution (Catic and Ploegh, 2005), we investigated the conservation of the ubiquitin signaling interactome from mouse to human. To this end, we matched homologs of identified ubiquitin interactors detected in mouse and human cells. Consistent with the analysis in ESCs and NPCs (Figure 3), interactors for K48, K63, and Met1 diUbs in ESCs and HeLa cells are strongly correlated (Figure S4A). Of the 302 significant interactors we could match in HeLa, ESCs, and NPCs, 128 (42%) showed cell-type-independent binding selectivity (Figure S4B). These conserved interactions show a similar binding pattern to diUbs in the different cell types (Figure S4C; Table S1). Strikingly, the majority of these interactors (~85%) selectively bind to K48, K63, or Met1 diUbs.

The NZF Domains of TAB2 and TAB3 Selectively Bind to K6 and K63 Linkages

Consistent with previous reports, we found that TAB2 and TAB3 selectively interact with K63 diUb (Kanayama et al., 2004; Kulathu et al., 2009; Sato et al., 2009b). Strikingly, however, we observed that all three TAB proteins (TAB1, TAB2, and TAB3) also bind strongly to K6 diUb (Figure S5A), and this was verified for TAB2 using immunoblotting (Figure 2C). To further investigate this observation, we expressed full-length or deletion mutants of TAB proteins in bacteria and used these proteins for in vitro binding assays. TAB1, which does not contain a predicted UBD, does not interact with diUb in vitro (data not shown), suggesting that the interaction between TAB1 and diUb is indirect. TAB2 and

Figure 2. Interactors for All diUb Linkages in HeLa Cells

(A) Schematic overview of the label-free UbIA-MS workflow to identify interactors for all diUbs.

(B) Hierarchical clustering of statistically significant interactors (rows) of the different diUbs (columns). Red indicates enrichment, whereas lack of enrichment is indicated in blue. Examples of known interactors for ubiquitin linkages are indicated on the left, whereas cluster numbers are indicated on the right.

(C) Immunoblotting-based validation experiments using antibodies against representative interactors (top). Black triangles indicate specific signals, whereas the red triangle indicates unspecific interaction with streptavidin beads. Bottom panel shows the respective enrichments for the interactors as identified by UbIA-MS.

(D) Representative enriched GO terms, including biological processes and protein complexes for the cluster identified in (B).

See also Figure S2 and Table S1.

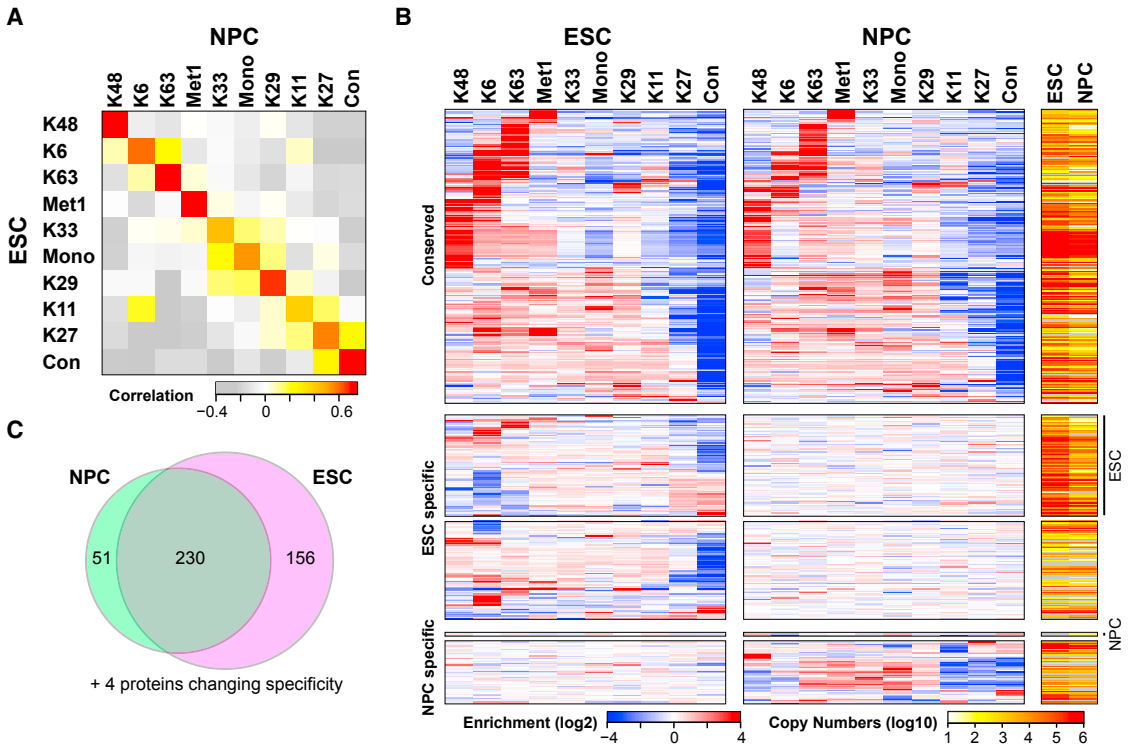

Figure 3. Cell-Type-Dependent and Independent diUb Interactors in ESCs and NPCs

(A) Correlation heatmap of the ESC and NPC diUb interactomes. Pairwise correlations of the enrichments of significant interactors between every diUb in ESCs and NPCs are plotted. Colors indicate anticorrelation (gray), no correlation (white), intermediate correlation (yellow), and strong correlation (red).

(B) Hierarchical clustering of significant interactors (rows) of the different diUbs (columns) identified in ESCs and NPCs. Analysis and colors as in Figure 2B. Heatmaps are shown for conserved (top), ESC-specific (middle), and NPC-specific (bottom) interactions. Copy numbers per cell of the interactors are indicated in the right columns, with values ranging from 10 (yellow) to 10^6 (red). ESC- and NPC-specific interactors that are significantly more abundant in ESCs and NPCs, respectively, are indicated on the right.

(C) Venn diagram showing overlap of significant interactors identified in ESCs and NPCs.

See also Figures S2–S4 and Table S1.

TAB3 both contain two UBDs, an N-terminal CUE domain and a C-terminal NZF domain (Kanayama et al., 2004). In vitro pull-downs failed to detect an interaction between the CUE domain and monoUb or any diUb (data not shown). However, we found that the NZF domains of TAB2 and TAB3 selectively interact with non-hydrolyzable and native K6 and K63 diUbs in vitro (Figure S5B). Consistent with our UbIA-MS and pull-down results, biolayer interferometry (BLI) experiments revealed that the NZF domain of TAB2 has a 4-fold higher binding affinity for K6 than for K63 diUb (Figures S2B and S5C). As a negative control, a low-affinity interaction between the TAB2 NZF domain and K48 diUb was observed.

To further investigate the ubiquitin linkage selectivity of the NZF domains of TAB proteins, we created expression plasmids containing four tandem TAB-NZF repeats. Purified GST-TAB-NZFs showed a clear binding preference for native K6 and K63 diUbs in vitro, although binding to other linkages was also observed (i.e., K11) (Figure S5D). Next, we purified TAB-NZFs from 293T cells stably expressing EGFP-TAB-NZFs using GFP affinity purification and quantified the enriched ubiquitin linkages using MS (Figure S5E). As a control, His-tagged ubiquitin was purified from 293T cells. It should be noted that the measured MS signals for different ubiquitin linkages does not necessarily reflect their absolute abundances, because different linkage-specific ubiquitin peptides may ionize with different efficiencies in MS. Nevertheless, whereas K6-linked ubiquitin is not detected in His-tagged ubiquitin purifications from 293T cells, this linkage represents 14% of the detected ubiquitin intensity in the TAB-NZFs pull-down, indicating that TAB-NZFs strongly enrich native K6 containing polyUb chains from cell extracts (Figure S5E). K63 and K11 linkages are also slightly enriched, which is consistent with the GST pull-down data.

The selective interactions between TAB proteins and K6 ubiquitin linkages have been overlooked in previous studies that have been limited to K48, K63, and Met1 linkages only (Kulathu et al., 2009; Sato et al., 2009b). Taken together, these results indicate that the NZF domains of TAB2 and TAB3 selectively interact with K6 and K63 ubiquitin linkages, which also implies that K6 polyUb may be involved in NF-κB signaling.

Linker Regions of tUIMs Define Linkage-Selective Avidity

Previous studies have shown that the formation of an α helix in the inter-UIM region, which positions both UIMs into the same

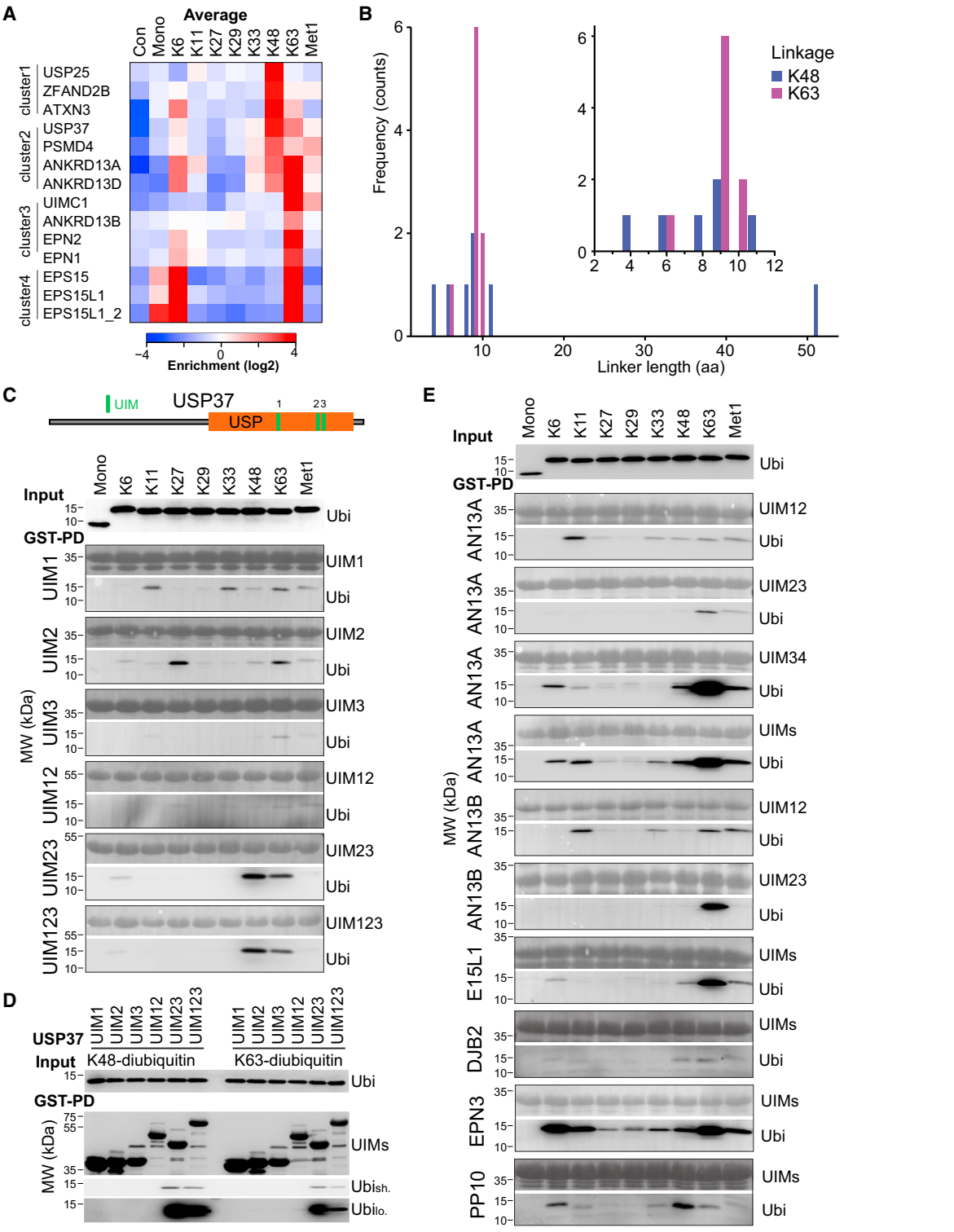

Figure 4. Inter-UIM Linker Regions Define Avid Binding to K48 and K63 diUbs

(A) Hierarchical clustering of UBPs with tUIMs identified in HeLa, ESCs, and NPCs. Enrichments are averages of HeLa, ESC, and NPC pull-downs. Analysis and colors as in Figure 2B. Interactors were clustered into four groups according to their binding selectivity to K6, K48 and K63 diUbs.

(B) Frequency plots of the length of inter-UIM region of identified interactors grouped by diUb selectivity. For UBPs with more than two UIMs (USP37 and ANKRD13B), linker regions of tUIMs that bind to K48 and K63 are shown.

(legend continued on next page)

orientation, is critical for selective K63 diUb recognition by UIMC1 (also known as RAP80) and EPN1 (Sato et al., 2009a; Sims and Cohen, 2009). The human and mouse genome encodes for 21 proteins containing UIMs as annotated in the SMART database, 5 of which contain only one UIM. In our data, 13 out of 16 UBPs containing tUIMs, including UIMC1 and EPN1, were shown to preferentially bind to K48 and/or K63 diUbs (Figures 4A and S6A). In contrast, UBPs containing only one UIM did not demonstrate obvious linkage selectivity (Figure S2K).

A few tUIMs containing UBPs selectively bind to K48 diUb, including the known K48 selective interactors ATXN3 and ZFAND2B (Sims and Cohen, 2009; Rahighi et al., 2016). Whereas the inter-UIM linker is fixed (9–10 aa) for K63 diUb selective interactors, the inter-UIM length of K48 diUb selective interactors is variable (Figures 4A, 4B, and S6B). To verify K48 linkage selective binding, we performed in vitro interaction assays for two DUBs, USP25 and USP37, and all diUbs. As a negative control, we made use of a glutathione S-transferase (GST)-only construct that displays no detectable affinity for monoUb or diUb (Figure S6C). As shown in Figures 4C, 4D, S6D, and S6E, two UIMs (UIM12 for USP25 and UIM23 for USP37) together are required for selective K48 diUb binding. This suggests that the inter-UIM region is necessary for selective binding of USP25 and USP37 to K48 diUb. In contrast to the MS and immunoblotting data, in which USP25 shows exclusive binding selectivity to K48 diUb (Figures 2C and S6A), recombinant tUIMs of USP25 also interact with K63 diUb (Figure S6D). This may be due to the fact that the in vitro binding validation assays were performed with truncated recombinant protein, while cofactors or PTMs in the context of the full-length protein may affect the binding selectivity of USP25 in mammalian cell lysates. The interaction between USP37 tUIMs and K63 linkages has been reported previously (Figure 4D) (Tanno et al., 2014). Further studies are required to explain how USP37 tUIMs binds to both K48 and K63 diUbs, considering the fact that K48 and K63 diUbs conformations are very different in solution.

In addition to UIMC1 and EPN1, we identified six other tUIMs containing UBPs that selectively bind to K63 diUb (Figure 4A, clusters 2, 3, and 4). Remarkably, four of them, namely ANKRD13A, ANKRD13D, EPN2, and ANKRD13B, have the same inter-UIM region length (9 aa) as UIMC1 (Figure S6B). This is in line with the conclusion that the length of the inter-UIM linker predicts K63 linkage selectivity. In vitro interaction assays indicated that the tUIM34 of ANKRD13A and tUIM23 of ANKRD13B, define the selectivity for K63 diUb (Figure 4E). Although EPS15 and EPS15L1 have different linker region lengths compared to that of UIMC1, the binding surfaces of UIM1 and UIM2 could still be positioned at the same side of the α helix, which allows binding to the two Ile44 patches of K63 diUb (Sato et al., 2009a). This is in concordance with a study that demonstrated that EPS15 has binding preference for K63 over K48 polyUb chains (Barriere et al., 2006). In addition, we showed that tUIMs of EPN3 and PAPR10, but not DNAJB2, which has a relatively long inter-UIM region, display avid binding to diUbs (Figure 4E). Taken together, our results support the theorem that the inter-UIM linker determines the avid binding to different ubiquitin linkages via arranging the positions of tUIMs (Sato et al., 2009a).

UCHL3 Regulates the Formation of K27 polyUb Chains In Vivo

In our UbIA-MS experiments, a number of DUBs were identified that display selective binding to certain diUbs (Figures 5A–5C). The observed binding selectivity for these DUBs is mainly cell-type independent (Figures 5A–5D). Some of these DUBs are known to cleave specific polyUb chains. For instance, ZRANB1 (TRABID), a DUB that hydrolyses K29 and K33 polyUb chains (Kristariyanto et al., 2015; Michel et al., 2015), binds selectively to these two diUbs in all three cell lines we screened. BRCC3, a component of BRCA1-A complex, which specifically hydrolases K63 polyUb chains, is highly enriched by K63 diUb in all three cell lines (Ritorto et al., 2014). In addition, we identified less studied DUBs with linkage-selective binding. For example, we identified USP32 as a K6 and K29 diUbs selective interactor, while USP19 selectively interacts with K29 diUb. Moreover, we identified two DUBs, UCHL3 and USP40, as selective K27 diUb interactors (Figure 5D).

Although a recent study has reported that K27 diUb is recognized by DNA damage response proteins, including RNF168 and UIMC1, previous studies as well as our results clearly indicate that RNF168 and UIMC1 selectively interact with K63 diUb (Figure 4A; Table S1) (Gatti et al., 2015; Thorslund et al., 2015). We decided to further investigate the detected selective interaction between UCHL3 and K27 diUb. We confirmed a direct interaction between UCHL3 and both non-hydrolyzable and native K27 diUb (Figures 5E and 5F). It should be noted that UCHL3 also interacts with monoUb and other diUbs, but to a much lesser extent (Figures 5A–5D). The binding affinity of UCHL3 for non-hydrolyzable and native K27 diUb was also determined by BLI experiments, with a K_D value of 131 ± 27.69 nM and 235 ± 78.82 nM, respectively (Figures 5G and 5H). Significant interactions with other diUbs could not be determined within the concentration range at which potent K27 diUb binding was observed (Figure S7A).

In line with previous studies, recombinant UCHL3 has no obvious DUB activity corresponding to any of the eight diUbs in vitro (Figure S7B, top) (Ritorto et al., 2014; Bett et al., 2015). In addition, UCHL3 purified from HEK293T cells showed no obvious in vitro DUB activity, although it cleaves polyubiquitinated lysozyme (Figure S7B, bottom) (Setsuie et al., 2010). To further investigate whether UCHL3 displays DUB activity toward

(C) In vitro interaction assay for a single UIM and combined UIMs of USP37. GST-tagged USP37 deletions coupled to glutathione agarose were incubated with biotin-tagged monoUb and diUb. Horseradish peroxidase (HRP)-streptavidin antibody was used to visualize interactions.
(D) tUIMs of USP37 (UIM2 and UIM3) enable selective binding to K48 and K63 diUbs in vitro. GST-tagged USP37 deletions coupled to glutathione agarose were incubated with biotin-tagged K48 and K63 diUbs. In vitro pull-down was performed as described in Figure 4C.
(E) Interaction assay for representative tUIMs and diUbs. In vitro pull-down was performed as described in (C).
See also Figure S6.

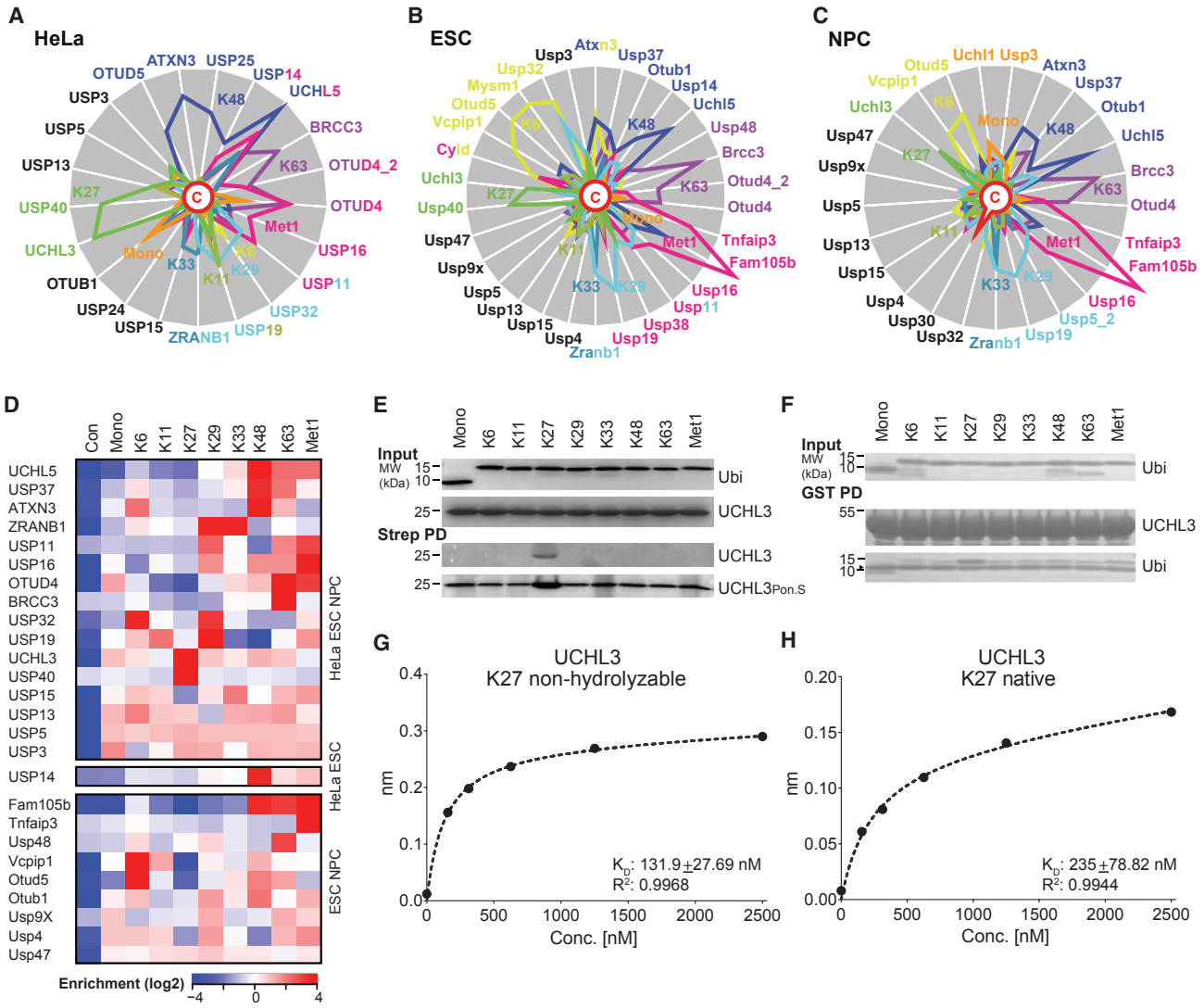

(legend on next page)

K27 ubiquitin linkages, we performed in vivo deubiquitination assays with a ubiquitin mutant in which all lysine residues are mutated to arginine except lysine K27. Intriguingly, UCHL3, but not USP40, which also selectively binds to K27 diUb, counteracts RNF168-induced K27 polyUb chain formation (Figure 5I) (Gatti et al., 2015). It should be noted that UCHL3 also inhibits formation of other polyUb chains, except K6 and K11 (Figure S7C). To investigate if the inhibitory effect of UCHL3 on K27 polyUb chain formation is caused by UCHL3 DUB activity, three mutants of UCHL3 were tested for their ability to counteract K27 polyUb chain formation (Misaghi et al., 2005). As shown in Figure 5J, mutating Cys95, the active-site nucleophile, abolishes the inhibitory effects of UCHL3 on RNF168-mediated formation of K27 polyUb chains, whereas mutating His169 or Asp184 has no obvious effect. This result implies that UCHL3 might act as a polyUb chain editing DUB through its active-site nucleophile, Cys95. Finally, we used an inducible UCHL3 small hairpin RNA (shRNA) construct to show that both basal and RNF168-induced K27 polyUb chain formation is potentiated upon depletion of UCHL3 in cells (Figure 5K).

Stimulus-Dependent Interactions of Ubiquitin Signaling

To investigate whether UbIA-MS is capable of identifying ubiquitin interaction dynamics upon cellular perturbation, we performed a K6 diUb interaction screening after induction of DNA damage in cells. K6 polyUb chains are known to play a role in the DNA damage response (Kulathu and Komander, 2012; Elia et al., 2015). HeLa cells were treated with doxorubicin for 6 hr, which results in an increase in phosphorylated H2AX (γ-H2AX) and monoubiquitinated γ-H2AX (Figure S7D). In total, 214 significant interactors (ANOVA thresholds were as follows: FDR = 0.001, S_0 = 2) were identified, which were grouped using k-means clustering (Figures 6A and S7E). Of the four ubiquitin interaction clusters, clusters 4, 6, and 7 represent interactors that do not show increased binding to monoUb or K6 diUb upon DNA damage (Figure 6A), indicating that the binding of these interactors is constitutive and not linked to the DNA damage response. Interestingly, interactors in cluster 1 bind with a higher affinity to monoUb and/or K6 diUb after doxorubicin treatment (Figures 6A and 6B). To investigate whether these binding dynamics are caused by changes in protein abundance after doxorubicin treatment, we quantified protein concentrations in the nuclear extracts (Figure 6B, right column; Table S1). Out of the 49 dynamic interactors in cluster 1, 10 are more abundant after doxorubicin treatment (>2-fold change). An example of this is UBR5, an E3 ligase that controls chromatin ubiquitination after DNA damage (Gudjonsson et al., 2012), which binds more potently to both baits after treatment but is also more abundant after treatment. Interestingly, we also identified five proteins with increased affinity to K6 diUb whose expression is not significantly altered upon doxorubicin treatment. One example of this is VCPIP1, a DUB whose activity is known to be regulated by phosphorylation during the cell cycle (Zhang and Wang, 2015). Therefore, it would be interesting to determine whether phosphorylation affects the interaction between VCPIP1 and K6 diUb. Furthermore, two known DNA-damage-related proteins, CDK7 and CDKN2A, preferentially bind to K6 diUb upon doxorubicin treatment. To further verify these observations, we made use of a proximity ligation assay (PLA), which is a microscopy-based assay that can be used to investigate whether two proteins of interest interact in vivo. As shown in Figures 6C and 6D, an interaction signal can be detected between CDK7, CDKN2A and K6 polyUb chains, but these signals are greatly stimulated upon induction of DNA damage (compare subpanels e and g in Figures 6C and 6D). These in vivo data are therefore in agreement with the in vitro quantitative MS data. Taken together, these results reveal stimulus-dependent interactions for monoUb and K6 diUb upon induction of DNA damage. In addition, in combination with protein abundance analysis, these interactions can be classified into protein-expression dependent and independent dynamic interactions.

Ubiquitin-Chain-Length-Dependent and Independent Interactions

In most of the interaction screenings presented thus far, we made use of chemical synthesized diUb. However, endogenous

Figure 5. UCHL3 Regulates K27 Polyubiquitination In Vivo

(A–C) Spider plots showing the detected binding preferences of DUBs to diUbs in HeLa cells (A), ESCs (B), and NPCs (C). All uppercase annotation is used to indicate DUBs identified in HeLa cells, while lowercase annotation indicates DUBs identified in mouse cell lines. The distance from the center indicates enrichment, ranging from 2^0 (center) to 2^8 (periphery).

(D) Hierarchical clustering of DUBs identified in HeLa cells, ESCs, and NPCs. Heatmaps of average enrichments are shown for DUBs in HeLa cells, ESCs, and NPCs (top); HeLa cells and ESCs (middle); and ESCs and NPCs (bottom). Analysis and colors are as in Figure 2B.

(E) UCHL3 shows binding selectivity to non-hydrolyzable K27 diUb in vitro. Biotin-tagged monoUbs and diUbs coupled to streptavidin agarose were incubated with recombinant UCHL3. Ponceau red staining and immunoblotting using a UCHL3 antibody were used to detect interaction.

(F) UCHL3 shows binding selectivity to native K27 diUb in vitro. GST-tagged UCHL3 coupled to glutathione Sepharose was incubated with native diUb. Coomassie brilliant blue G-250 was used to stain the SDS-PAGE gel to detect interactions. The triangle indicates a nonspecific band. Note that K6, K48, and K63 diUbs are contaminated with monoUb.

(G and H) Binding isotherm of UCHL3 with K27 non-hydrolyzable (G) and native (H) diUb measured using BLI. N-terminally biotinylated non-hydrolyzable (G) and amine biotinylated native (H) K27 diUb was immobilized on a streptavidin coated biosensor and measured with increasing concentrations of UCHL3. Binding constants were determined using non-linear regression least-squares fit.

(I) UCHL3 impairs RNF168-induced K27 polyUb chain formation in vivo. HEK293T cells were transfected with indicated plasmids for 48 hr. In vivo K27 polyUb chains were enriched from lysates by nickel agarose beads. Hemagglutinin (HA) antibody was used to detect K27 polyUb chains.

(J) Cysteine 95 is the DUB active site of UCHL3. In vivo deubiquitination assay was performed as described in (I).

(K) Impairment of UCHL3 expression potentiates K27 polyUb chain formation in vivo. HEK293T cells stably expressing an inducible shRNA against UCHL3 were transfected with the indicated plasmids. Doxycycline was added at 1 μg/mL for 3 days before harvesting the cells. In vivo deubiquitination assay was then performed as described in (I).

See also Figure S7.

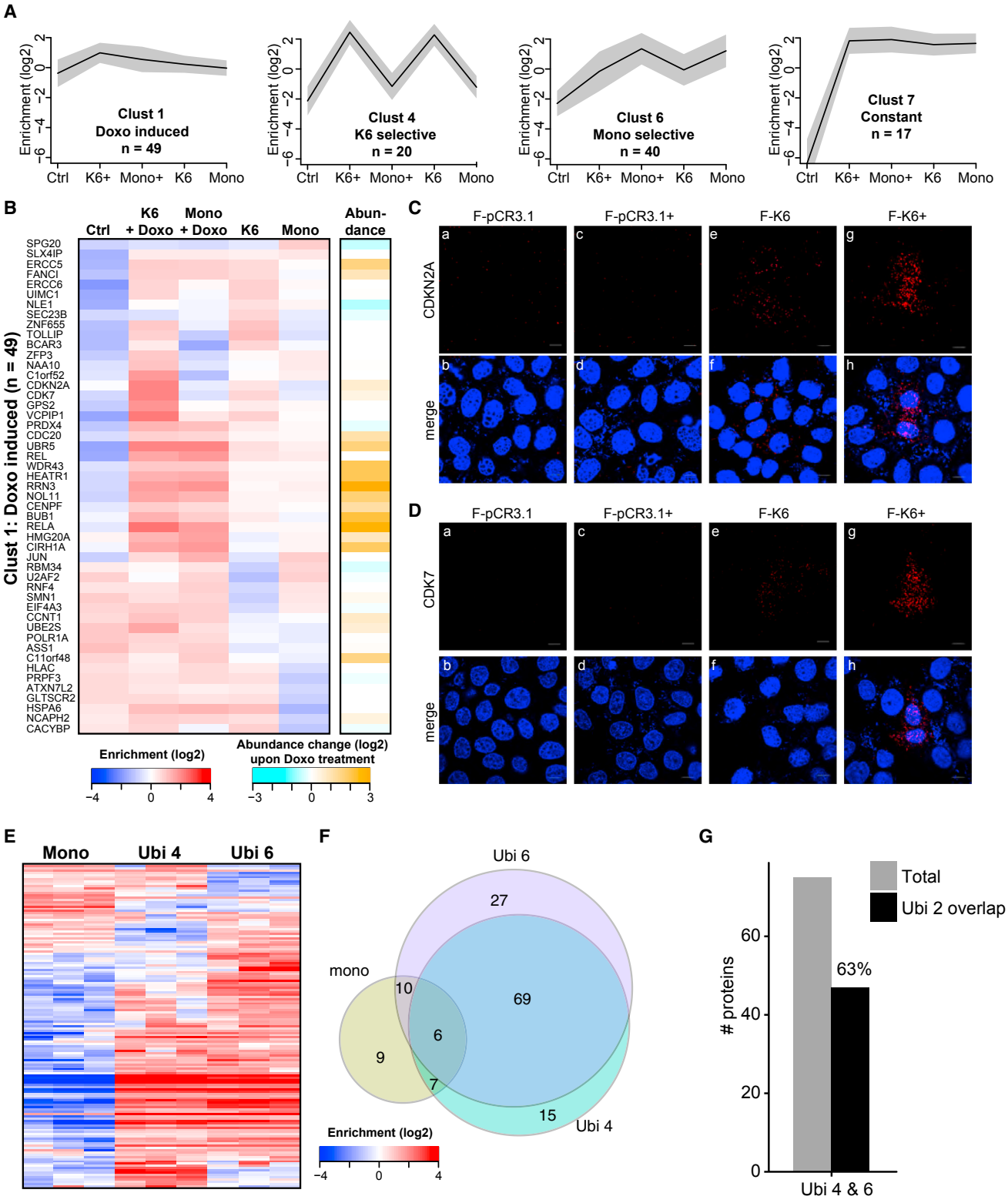

Figure 6. Ubiquitin Interactions upon DNA Damage Induction and for Different polyUb Chain Lengths

(A) K-means clustering of monoUb and K6 diUb interactors with or without doxorubicin treatment. Black line indicates the mean enrichment, and gray shading indicates the SD. See Figure S7E for the three clusters containing background proteins.

(legend continued on next page)

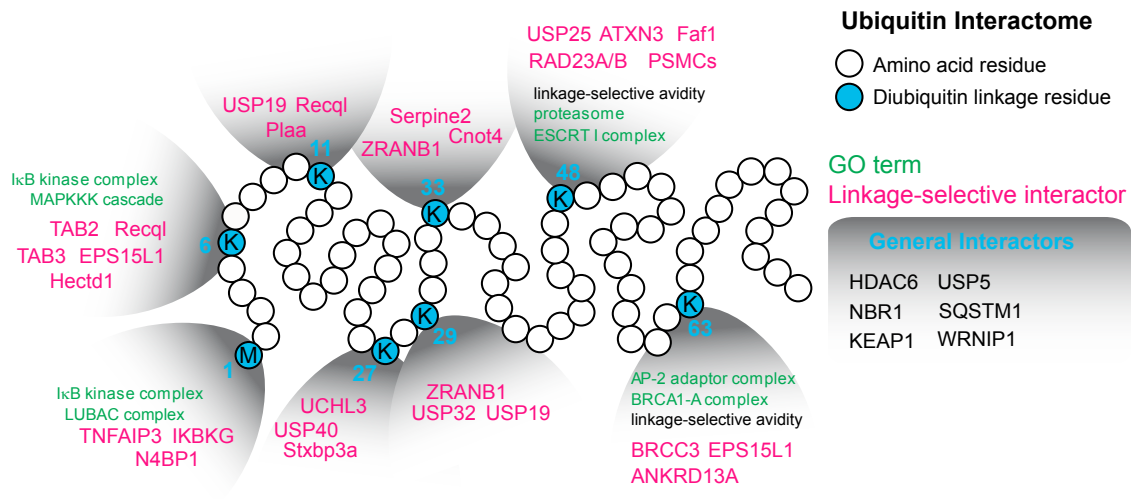

Figure 7. An Interaction Landscape of Ubiquitin Signaling

Overview figure showing representative interactors for different diUbs and related GO terms. Linkage-independent and monoUb interactors are listed on the right.

ubiquitin linkages can exist in longer forms. To investigate whether polyUb chain lengths affect interactions, we performed UbIA-MS with linear tetra- and hexa-ubiquitin chains in HeLa whole-cell extracts. As shown in Figures 6E and 6F, interactions for linear tetra- and hexa-ubiquitin chain show a large degree of overlap (75 out of 137 proteins [56%]). Moreover, 63% of the interactors that bind to both linear tetra- and hexa-ubiquitin chains had previously also been identified as linear diUb interactors (Figure 6G). Altogether, these results reveal that the majority of linear ubiquitin chain interactors display chain-length-independent interaction dynamics.

DISCUSSION

Although it is generally appreciated that UBPs play an important role as effectors of ubiquitin signaling, tools and methods to identify UBPs for all ubiquitin linkages in an unbiased, proteome-wide manner have thus far not been available. Here, we have developed UbIA-MS, a sensitive, robust, and reproducible MS-based interaction proteomics workflow to identify interactors for ubiquitin signaling in an unbiased manner (Figure 7). The interaction landscape for ubiquitin signaling that we present here is, however, by no means exhaustive. We have mainly studied interactions with diUb in a few steady-state asynchronously growing cell types. Longer, branched and heterotypical polyUb chains are formed in vivo, and each of these different polyUb chains may serve as a binding scaffold for different effector proteins. The interaction landscape presented here therefore most likely only represents the tip of the iceberg of the complete interaction landscape of ubiquitin signaling. This hypothesis is further supported by the experiments shown in Figure 6, which indicate that interactions with ubiquitin chains can be induced upon cellular perturbation (induction of DNA damage). Furthermore, interactions with ubiquitin are, at least to some extent, affected by ubiquitin chain length. In the future, UbIA-MS will serve as a powerful tool to decipher interactions with a variety of different ubiquitin linkages in different biological contexts and with different ubiquitin lengths and topologies.

Interestingly, our results suggest that some ubiquitin linkages (mainly K48, K63, and Met1) tend to recruit cell-type-independent interactors. This observation suggests that these constitutive interactors and associated ubiquitin linkages are more likely to be involved in "housekeeping" functions, which are required for normal cellular homeostasis. A good example is NF-κB signaling, which is tightly regulated by K63 and Met1 polyUb and is required for cells to respond to stimuli such as stress, inflammation, and infection (Liu and Chen, 2011). Interestingly, although some cell-type-specific ubiquitin interactions can be explained by differences in protein abundance between different cell types, some interactors display cell-type-specific ubiquitin binding selectivity in the absence of obvious expression changes. These cell-type-specific, expression-independent differential ubiquitin linkage interactions might be explained by additional PTMs or certain cell-type-specific interacting partners

(B) Hierarchical clustering of the interactions in cluster 1 of (A). Analysis and colors are as in Figure 2B. Change of protein abundance is shown in the right column. Orange indicates increased abundance, whereas cyan indicates decreased abundance.

(C and D) PLA to detect the interactions of K6 polyUb chains and endogenous proteins. HeLa cells transiently transfected with empty vector (a–d) or FLAG-K6 (e–h) were stained with antibodies against FLAG and CDKN2A (C) or FLAG and CDK7 (D). Cells were also stained with DAPI to visualize cell nuclei (in blue, shown in merge panels). + indicates treatment with doxorubicin. Scale bar, 10 μm. One representative picture is shown for all conditions.

(E) Hierarchical clustering of the interactors (rows) of linear tetra- and hexa-ubiquitin (columns). Analysis and colors are as in Figure 2B.

(F) Venn diagram showing overlap of significant interactors identified using linear tetra- and hexa-ubiquitin chains.

(G) Bar graph showing overlap of significant Met1 linkages interactors identified in Figures 2B and (E).

See also Figure S7 and Table S1.

that are involved in regulating cell-type-specific, linkage-selective ubiquitin interactions.

Many DUBs covered in our datasets display cell-type-independent, linkage-selective diUb binding. In many cases, the observed binding selectivity of DUBs is in good agreement with their known ubiquitin cleavage specificity. However, for some DUBs, the detected linkage-selective binding does not correlate well with their known cleavage specificity. One example is Tnfaip3 (also known as A20), which displays selective binding to linear diUb in our screens (Figure 5D). This observation is in good agreement with previous in vitro analyses, which revealed that the A20 protein binds with a much higher affinity to linear diUb than to K63 diUb (Wertz et al., 2015). However, the A20 protein shows no detectable cleavage activity toward Met1 linkage, but it cleaves K63 linkage very efficiently (Tokunaga et al., 2012). Another example from our own data is UCHL3, which cleaves multiple linkages in vivo but displays selective binding to K27 diUb. We speculate that the observed difference in ubiquitin linkage binding and cleavage activity of some DUBs might be particularly relevant for the selective recognition and/or subsequent cleavage of heterotypic polyUb chains in vivo.

STAR★METHODS

Detailed methods are provided in the online version of this paper and include the following:

- KEY RESOURCES TABLE
- CONTACT FOR REAGENT AND RESOURCE SHARING
- EXPERIMENTAL MODEL AND SUBJECT DETAILS
- METHOD DETAILS
  - Cell culture and extract preparation
  - SILAC-based ubiquitin pull-down
  - In-gel and on-bead digestion
  - Synthesis of non-hydrolyzable diubiquitin
  - Label free pull-down
  - Recombinant protein purification
  - In vitro interaction assay
  - Affinity and kinetic measurements with BLI
  - Enrichment of cellular ubiquitin linkages by the TAB NZF domain
  - In vitro and in vivo deubiquitination assay
  - Proximity ligation assay (PLA)
  - Global absolute protein quantification
  - Mass spectrometry analysis
- QUANTIFICATION AND STATISTICAL ANALYSIS
  - BLI data analysis
  - Mass spectrometry data analysis
- DATA AND SOFTWARE AVAILABILITY
  - Software
  - Data Resources

SUPPLEMENTAL INFORMATION

Supplemental Information includes seven figures and one table and can be found with this article online at http://dx.doi.org/10.1016/j.molcel.2017.01.004.

AUTHOR CONTRIBUTIONS

X.Z. and M.V. conceived the project and wrote the manuscript, with input from A.H.S., H.O., and G.B.A.v.T., and X.Z. performed most of the experiments. A.H.S. analyzed the MS data and made related figures. G.B.A.v.T. designed and synthesized non-hydrolyzable and native diubiquitin reagents and performed the Biolayer interferometry experiments. P.W.T.C.J. and M.M.M. measured the MS samples. M.V. and H.O. supervised the project.

ACKNOWLEDGMENTS

We like to thank Cristina Furlan for help with endogenous ubiquitin linkages identification, Remco Merkx for help with the synthesis of α-azido-(L)-norleucine, Dris el Atmioui and Duco van Dalen for the ubiquitin synthesis, and Gerbrand J. van der Heden van Noort for synthetic advice. We like to thank Microscopic Imaging Centre of Radboud Institute for Molecular Life Sciences for confocal imaging. We would like to thank Wiep K. Smits and the LUMC Experimental Bacteriology department for use of the Octet96 BLI system. We would like to thank all members of the Vermeulen and Ovaa labs for fruitful discussions. Work in the Vermeulen lab is supported by NWO Gravitation program CGC.nl. Work in the Ovaa lab is supported by ERC grant Ubicode (nr. 281699). H.O. is a shareholder in the biotech company UbiQ.

Received: June 13, 2016
Revised: December 6, 2016
Accepted: January 5, 2017
Published: February 9, 2017

REFERENCES

Barriere, H., Nemes, C., Lechardeur, D., Khan-Mohammad, M., Fruh, K., and Lukacs, G.L. (2006). Molecular basis of oligoubiquitin-dependent internalization of membrane proteins in mammalian cells. Traffic *7*, 282–297.

Bett, J.S., Ritorto, M.S., Ewan, R., Jaffray, E.G., Virdee, S., Chin, J.W., Knebel, A., Kurz, T., Trost, M., Tatham, M.H., and Hay, R.T. (2015). Ubiquitin C-terminal hydrolases cleave isopeptide- and peptide-linked ubiquitin from structured proteins but do not edit ubiquitin homopolymers. Biochem. J. *466*, 489–498.

Catic, A., and Ploegh, H.L. (2005). Ubiquitin—conserved protein or selfish gene? Trends Biochem. Sci. *30*, 600–604.

Cohen, P. (2014). Immune diseases caused by mutations in kinases and components of the ubiquitin system. Nat. Immunol. *15*, 521–529.

Cooper, E.M., Cutcliffe, C., Kristiansen, T.Z., Pandey, A., Pickart, C.M., and Cohen, R.E. (2009). K63-specific deubiquitination by two JAMM/MPN+ complexes: BRISC-associated Brcc36 and proteasomal Poh1. EMBO J. *28*, 621–631.

Cox, J., and Mann, M. (2008). MaxQuant enables high peptide identification rates, individualized p.p.b.-range mass accuracies and proteome-wide protein quantification. Nat. Biotechnol. *26*, 1367–1372.

Cox, J., and Mann, M. (2012). 1D and 2D annotation enrichment: a statistical method integrating quantitative proteomics with complementary high-throughput data. BMC Bioinformatics *13* (*Suppl 16*), S12.

Eger, S., Scheffner, M., Marx, A., and Rubini, M. (2010). Synthesis of defined ubiquitin dimers. J. Am. Chem. Soc. *132*, 16337–16339.

Ekkebus, R., van Kasteren, S.I., Kulathu, Y., Scholten, A., Berlin, I., Geurink, P.P., de Jong, A., Goerdayal, S., Neefjes, J., Heck, A.J.R., et al. (2013). On terminal alkynes that can react with active-site cysteine nucleophiles in proteases. J. Am. Chem. Soc. *135*, 2867–2870.

El Oualid, F., Merkx, R., Ekkebus, R., Hameed, D.S., Smit, J.J., de Jong, A., Hilkmann, H., Sixma, T.K., and Ovaa, H. (2010). Chemical synthesis of ubiquitin, ubiquitin-based probes, and diubiquitin. Angew. Chem. Int. Ed. Engl. *49*, 10149–10153.

Elia, A.E.H., Boardman, A.P., Wang, D.C., Huttlin, E.L., Everley, R.A., Dephoure, N., Zhou, C., Koren, I., Gygi, S.P., and Elledge, S.J. (2015). Quantitative proteomic atlas of ubiquitination and acetylation in the DNA damage response. Mol. Cell *59*, 867–881.

Emmerich, C.H., Ordureau, A., Strickson, S., Arthur, J.S.C., Pedrioli, P.G.A., Komander, D., and Cohen, P. (2013). Activation of the canonical IKK complex by K63/M1-linked hybrid ubiquitin chains. Proc. Natl. Acad. Sci. USA *110*, 15247–15252.

Flierman, D., van der Heden van Noort, G.J., Ekkebus, R., Geurink, P.P., Mevissen, T.E.T., Hospenthal, M.K., Komander, D., and Ovaa, H. (2016). Non-hydrolyzable diubiquitin probes reveal linkage-specific reactivity of deubiquitylating enzymes mediated by S2 pockets. Cell Chem. Biol. *23*, 472–482.

Gatti, M., Pinato, S., Maiolica, A., Rocchio, F., Prato, M.G., Aebersold, R., and Penengo, L. (2015). RNF168 promotes noncanonical K27 ubiquitination to signal DNA damage. Cell Rep. *10*, 226–238.

Grice, G.L., Lobb, I.T., Weekes, M.P., Gygi, S.P., Antrobus, R., and Nathan, J.A. (2015). The proteasome distinguishes between heterotypic and homotypic lysine-11-linked polyubiquitin chains. Cell Rep. *12*, 545–553.

Gudjonsson, T., Altmeyer, M., Savic, V., Toledo, L., Dinant, C., Grøfte, M., Bartkova, J., Poulsen, M., Oka, Y., Bekker-Jensen, S., et al. (2012). TRIP12 and UBR5 suppress spreading of chromatin ubiquitylation at damaged chromosomes. Cell *150*, 697–709.

Herhaus, L., and Dikic, I. (2015). Expanding the ubiquitin code through post-translational modification. EMBO Rep. *16*, 1071–1083.

Herold, M.J., van den Brandt, J., Seibler, J., and Reichardt, H.M. (2008). Inducible and reversible gene silencing by stable integration of an shRNA-encoding lentivirus in transgenic rats. Proc. Natl. Acad. Sci. USA *105*, 18507–18512.

Husnjak, K., and Dikic, I. (2012). Ubiquitin-binding proteins: decoders of ubiquitin-mediated cellular functions. Annu. Rev. Biochem. *81*, 291–322.

Iwai, K., Fujita, H., and Sasaki, Y. (2014). Linear ubiquitin chains: NF-κB signalling, cell death and beyond. Nat. Rev. Mol. Cell Biol. *15*, 503–508.

Kanayama, A., Seth, R.B., Sun, L., Ea, C.-K., Hong, M., Shaito, A., Chiu, Y.-H., Deng, L., and Chen, Z.J. (2004). TAB2 and TAB3 activate the NF-kappaB pathway through binding to polyubiquitin chains. Mol. Cell *15*, 535–548.

Komander, D., and Rape, M. (2012). The ubiquitin code. Annu. Rev. Biochem. *81*, 203–229.

Kristariyanto, Y.A., Abdul Rehman, S.A., Campbell, D.G., Morrice, N.A., Johnson, C., Toth, R., and Kulathu, Y. (2015). K29-selective ubiquitin binding domain reveals structural basis of specificity and heterotypic nature of k29 polyubiquitin. Mol. Cell *58*, 83–94.

Kulathu, Y., and Komander, D. (2012). Atypical ubiquitylation—the unexplored world of polyubiquitin beyond Lys48 and Lys63 linkages. Nat. Rev. Mol. Cell Biol. *13*, 508–523.

Kulathu, Y., Akutsu, M., Bremm, A., Hofmann, K., and Komander, D. (2009). Two-sided ubiquitin binding explains specificity of the TAB2 NZF domain. Nat. Struct. Mol. Biol. *16*, 1328–1330.

Kumar, K.S.A., Spasser, L., Erlich, L.A., Bavikar, S.N., and Brik, A. (2010). Total chemical synthesis of di-ubiquitin chains. Angew. Chem. Int. Ed. Engl. *49*, 9126–9131.

Larsen, C.N., Price, J.S., and Wilkinson, K.D. (1996). Substrate binding and catalysis by ubiquitin C-terminal hydrolases: identification of two active site residues. Biochemistry *35*, 6735–6744.

Letunic, I., Doerks, T., and Bork, P. (2015). SMART: recent updates, new developments and status in 2015. Nucleic Acids Res. *43*, D257–D260.

Licchesi, J.D.F., Mieszczanek, J., Mevissen, T.E.T., Rutherford, T.J., Akutsu, M., Virdee, S., El Oualid, F., Chin, J.W., Ovaa, H., Bienz, M., and Komander, D. (2011). An ankyrin-repeat ubiquitin-binding domain determines TRABID's specificity for atypical ubiquitin chains. Nat. Struct. Mol. Biol. *19*, 62–71.

Lim, K.-L., Chew, K.C.M., Tan, J.M.M., Wang, C., Chung, K.K.K., Zhang, Y., Tanaka, Y., Smith, W., Engelender, S., Ross, C.A., et al. (2005). Parkin mediates nonclassical, proteasomal-independent ubiquitination of synphilin-1: implications for Lewy body formation. J. Neurosci. *25*, 2002–2009.

Liu, S., and Chen, Z.J. (2011). Expanding role of ubiquitination in NF-κB signaling. Cell Res. *21*, 6–21.

Meyer, H.-J., and Rape, M. (2014). Enhanced protein degradation by branched ubiquitin chains. Cell *157*, 910–921.

Michel, M.A., Elliott, P.R., Swatek, K.N., Simicek, M., Pruneda, J.N., Wagstaff, J.L., Freund, S.M.V., and Komander, D. (2015). Assembly and specific recognition of k29- and k33-linked polyubiquitin. Mol. Cell *58*, 95–109.

Misaghi, S., Galardy, P.J., Meester, W.J.N., Ovaa, H., Ploegh, H.L., and Gaudet, R. (2005). Structure of the ubiquitin hydrolase UCH-L3 complexed with a suicide substrate. J. Biol. Chem. *280*, 1512–1520.

Moss, N., Xiong, Z., Burke, M., Cogan, D., Gao, D.A., Haverty, K., Heim-Riether, A., Hickey, E.R., Nagaraja, R., Netherton, M., et al. (2012). Exploration of cathepsin S inhibitors characterized by a triazole P1-P2 amide replacement. Bioorg. Med. Chem. Lett. *22*, 7189–7193.

Nagaraj, N., Wisniewski, J.R., Geiger, T., Cox, J., Kircher, M., Kelso, J., Pääbo, S., and Mann, M. (2011). Deep proteome and transcriptome mapping of a human cancer cell line. Mol. Syst. Biol. *7*, 548.

Peng, J., Schwartz, D., Elias, J.E., Thoreen, C.C., Cheng, D., Marsischky, G., Roelofs, J., Finley, D., and Gygi, S.P. (2003). A proteomics approach to understanding protein ubiquitination. Nat. Biotechnol. *21*, 921–926.

Rahighi, S., Ikeda, F., Kawasaki, M., Akutsu, M., Suzuki, N., Kato, R., Kensche, T., Uejima, T., Bloor, S., Komander, D., et al. (2009). Specific recognition of linear ubiquitin chains by NEMO is important for NF-kappaB activation. Cell *136*, 1098–1109.

Rahighi, S., Braunstein, I., Ternette, N., Kessler, B., Kawasaki, M., Kato, R., Matsui, T., Weiss, T.M., Stanhill, A., and Wakatsuki, S. (2016). Selective binding of AIRAPL tandem UIMs to Lys48-linked tri-ubiquitin chains. Structure *24*, 412–422.

Reyes-Turcu, F.E., Horton, J.R., Mullally, J.E., Heroux, A., Cheng, X., and Wilkinson, K.D. (2006). The ubiquitin binding domain ZnF UBP recognizes the C-terminal diglycine motif of unanchored ubiquitin. Cell *124*, 1197–1208.

Ritorto, M.S., Ewan, R., Perez-Oliva, A.B., Knebel, A., Buhrlage, S.J., Wightman, M., Kelly, S.M., Wood, N.T., Virdee, S., Gray, N.S., et al. (2014). Screening of DUB activity and specificity by MALDI-TOF mass spectrometry. Nat. Commun. *5*, 4763.

Sato, Y., Yoshikawa, A., Mimura, H., Yamashita, M., Yamagata, A., and Fukai, S. (2009a). Structural basis for specific recognition of Lys 63-linked polyubiquitin chains by tandem UIMs of RAP80. EMBO J. *28*, 2461–2468.

Sato, Y., Yoshikawa, A., Yamashita, M., Yamagata, A., and Fukai, S. (2009b). Structural basis for specific recognition of Lys 63-linked polyubiquitin chains by NZF domains of TAB2 and TAB3. EMBO J. *28*, 3903–3909.

Schwanhäusser, B., Busse, D., Li, N., Dittmar, G., Schuchhardt, J., Wolf, J., Chen, W., and Selbach, M. (2011). Global quantification of mammalian gene expression control. Nature *473*, 337–342.

Setsuie, R., Suzuki, M., Tsuchiya, Y., and Wada, K. (2010). Skeletal muscles of Uchl3 knockout mice show polyubiquitinated protein accumulation and stress responses. Neurochem. Int. *56*, 911–918.

Sims, J.J., and Cohen, R.E. (2009). Linkage-specific avidity defines the lysine 63-linked polyubiquitin-binding preference of rap80. Mol. Cell *33*, 775–783.

Smits, A.H., and Vermeulen, M. (2016). Characterizing protein-protein interactions using mass spectrometry: challenges and opportunities. Trends Biotechnol. *34*, 825–834.

Smits, A.H., Jansen, P.W.T.C., Poser, I., Hyman, A.A., and Vermeulen, M. (2013). Stoichiometry of chromatin-associated protein complexes revealed by label-free quantitative mass spectrometry-based proteomics. Nucleic Acids Res. *41*, e28.

Spruijt, C.G., Gnerlich, F., Smits, A.H., Pfaffeneder, T., Jansen, P.W.T.C., Bauer, C., Münzel, M., Wagner, M., Müller, M., Khan, F., et al. (2013). Dynamic readers for 5-(hydroxy)methylcytosine and its oxidized derivatives. Cell *152*, 1146–1159.

Tanno, H., Shigematsu, T., Nishikawa, S., Hayakawa, A., Denda, K., Tanaka, T., and Komada, M. (2014). Ubiquitin-interacting motifs confer full catalytic activity, but not ubiquitin chain substrate specificity, to deubiquitinating enzyme USP37. J. Biol. Chem. *289*, 2415–2423.

Thorslund, T., Ripplinger, A., Hoffmann, S., Wild, T., Uckelmann, M., Villumsen, B., Narita, T., Sixma, T.K., Choudhary, C., Bekker-Jensen, S., and Mailand, N. (2015). Histone H1 couples initiation and amplification of ubiquitin signalling after DNA damage. Nature *527*, 389–393.

Tokunaga, F., Nishimasu, H., Ishitani, R., Goto, E., Noguchi, T., Mio, K., Kamei, K., Ma, A., Iwai, K., and Nureki, O. (2012). Specific recognition of linear polyubiquitin by A20 zinc finger 7 is involved in NF-κB regulation. EMBO J. *31*, 3856–3870.

Vizcaíno, J.A., Csordas, A., del-Toro, N., Dianes, J.A., Griss, J., Lavidas, I., Mayer, G., Perez-Riverol, Y., Reisinger, F., Ternent, T., et al. (2016). 2016 update of the PRIDE database and its related tools. Nucleic Acids Res. *44* (D1), D447–D456.

Weikart, N.D., Sommer, S., and Mootz, H.D. (2012). Click synthesis of ubiquitin dimer analogs to interrogate linkage-specific UBA domain binding. Chem. Commun. (Camb.) *48*, 296–298.

Wertz, I.E., Newton, K., Seshasayee, D., Kusam, S., Lam, C., Zhang, J., Popovych, N., Helgason, E., Schoeffler, A., Jeet, S., et al. (2015). Phosphorylation and linear ubiquitin direct A20 inhibition of inflammation. Nature *528*, 370–375.

Wiśniewski, J.R., Zougman, A., Nagaraj, N., and Mann, M. (2009). Universal sample preparation method for proteome analysis. Nat. Methods *6*, 359–362.

Xu, G., Paige, J.S., and Jaffrey, S.R. (2010). Global analysis of lysine ubiquitination by ubiquitin remnant immunoaffinity profiling. Nat. Biotechnol. *28*, 868–873.

Zhang, X., and Wang, Y. (2015). Cell cycle regulation of VCIP135 deubiquitinase activity and function in p97/p47-mediated Golgi reassembly. Mol. Biol. Cell *26*, 2242–2251.

Zhang, X., Zhang, J., Bauer, A., Zhang, L., Selinger, D.W., Lu, C.X., and Ten Dijke, P. (2013a). Fine-tuning BMP7 signalling in adipogenesis by UBE2O/E2-230K-mediated monoubiquitination of SMAD6. EMBO J. *32*, 996–1007.

Zhang, X., Zhang, J., Zhang, L., van Dam, H., and ten Dijke, P. (2013b). UBE2O negatively regulates TRAF6-mediated NF-κB activation by inhibiting TRAF6 polyubiquitination. Cell Res. *23*, 366–377.

Zhou, Z., and Fahrni, C.J. (2004). A fluorogenic probe for the copper(I)-catalyzed azide-alkyne ligation reaction: modulation of the fluorescence emission via 3(n,π)-1(π,π) inversion. J. Am. Chem. Soc. *126*, 8862–8863.

STAR★METHODS

KEY RESOURCES TABLE

REAGENT OR RESOURCE	SOURCE	IDENTIFIER
Antibodies		
Oct-3/4	Santa Cruz Biotechnology	Cat#sc-5279 RRID: AB_628051
Nanog	eBioscience	Cat#14-5761-80 RRID: AB_763613
Nestin	BD Biosciences	Cat#556309 RRID: AB_396354
MBD3	Santa Cruz Biotechnology	Cat#sc-9402 RRID: AB_2139757
ACTL8	Proteintech Group	Cat#17312-1-AP
HDAC6	Proteintech Group	Cat#12834-1-AP RRID: AB_10597094
NEMO/IKBKG	Santa Cruz Biotechnology	Cat#sc-8330 RRID: AB_2124846
MYCBP	Proteintech Group	Cat#12022-1-AP RRID: AB_2148722
RAD23A	Proteintech Group	Cat#11364-1-AP RRID: AB_2176739
BRE	Proteintech Group	Cat#11702-1-AP RRID: AB_2066049
ATXN3	Proteintech Group	Cat#13505-1-AP RRID: AB_2061192
UCHL3	Proteintech Group	Cat#12384-1-AP RRID: AB_2210915
EPS15L1	Proteintech Group	Cat#21243-1-AP RRID: AB_10733643
USP19	Proteintech Group	Cat#25768-1-AP
ADRM1	Proteintech Group	Cat#11468-1-AP RRID: AB_2273873
TAB2	Proteintech Group	Cat#14410-1-AP RRID: AB_2281638
USP25	Proteintech Group	Cat#12199-1-AP RRID: AB_2212771
Flag-tag	Sigma-Aldrich	Cat#F3165 RRID: AB_259529
Myc-tag	Santa Cruz Biotechnology	Cat#sc-789 RRID: AB_631274
HA-tag	Santa Cruz Biotechnology	Cat#sc-805 RRID: AB_631618
ACTIN	Sigma-Aldrich	Cat#A5441 RRID: AB_476744
GFP	Abcam	Cat#ab290 RRID: AB_303395
GFP	Santa Cruz Biotechnology	Cat# sc-8334 RRID: AB_641123
CDKN2A	Bethyl	Cat#A301-267A RRID: AB_890617
CDK7	Bethyl	Cat#A300-405A RRID: AB_2275973
HRP-streptavidin antibody	Thermo Fisher Scientific	Cat#PA1-26848 RRID: AB_795453
Chemicals, Peptides, and Recombinant Proteins		
Doxorubicin	Sigma-Aldrich	Cat #D1515, CAS: 25316-40-9
Polybrene	Sigma-Aldrich	Cat#107689, CAS: 28728-55-4
Puromycin	Sigma-Aldrich	Cat#7130, CAS: 58-60-6
Imidazole	Sigma-Aldrich	Cat#I5513, CAS: 288-32-4
N-Ethylmaleimide	Sigma-Aldrich	Cat#E3876, CAS: 128-53-0
IPTG	Promega	Cat#V3951
Glutathione	Chem-IMPEX	Cat#00159, CAS: 70-18-8
Formaldehyde	Merck Millipore	Cat#104003
Ammonium bicarbonate	Sigma-Aldrich	Cat# 09830, CAS: 1066-33-7
Iodoacetamide	Sigma-Aldrich	Cat#I1149, CAS: 144-48-9
Biotin	Sigma-Aldrich	Cat#B4501, CAS: 58-85-5
EZ-Link NHS-LC-LC-Biotin	Thermo Fisher Scientific	Cat#21343
CuSO4	Sigma-Aldrich	Cat#C8027, CAS:7758-99-8
sodium ascorbate	Sigma-Aldrich	Cat#PHR1279, CAS: 134-03-2
8-(Fmoc amino)-3,6-dioxaoctanoic acid	AK Scientific	Cat#166108-71-0, CAS:166108-71-0
Fmoc-L-δ-azidoornithine	Sigma-Aldrich	Cat#714291, CAS: 1097192-04-5

(*Continued on next page*)

Continued

REAGENT OR RESOURCE	SOURCE	IDENTIFIER
2-Chloroacetamide	Sigma-Aldrich	Cat#C0267, CAS: 79-07-2
Trypsin	Promega	Cat#V5280
3 × Flag peptide	APExBIO	Cat#A6001
DNase I	Sigma-Aldrich	Cat#000000004716728001
Factor Xa	New England BioLabs	Cat#P8010
Thrombin	GE healthcare Life Sciences	Cat#27-0846-01
6 × His-Ubiquitin	Ubiquitin-Proteasome Biotechnologies	Cat#E1301
6 × His-Non-cleavable Linear UB_4	Ubiquitin-Proteasome Biotechnologies	Cat#D4430
6 × His-Non-cleavable Linear UB_6	Ubiquitin-Proteasome Biotechnologies	Cat#D4410
Linear polyUB Chain-binding Protein Identification Kit	Ubiquitin-Proteasome Biotechnologies	Cat#J2520
$Ubiquitin_{1-75}$ and $Ubiquitin_{1-76}$	El Oualid et al., 2010	N/A
Biotin-PEG-Ub_{1-75}PA	This paper	N/A
Ub_{1-76} –N3 precursors	This paper	N/A
Biotin tagged non-hydrolyzable diubiquitins	This paper	N/A
Di-ubiquitin Explorer Kit	Ubiquitin-Proteasome Biotechnologies	Cat#J2000
Homemade native diubiquitins	El Oualid et al., 2010	N/A
Biotinylated native diubiquitins	This paper	N/A
UCHL3	Larsen et al., 1996	N/A
GST-tagged recombinant proteins	This paper see below recombinant DNA	N/A
Critical Commercial Assays		
Proximity ligation assay	Sigma-Aldrich	Cat#DUO92101
SliverQuest Silver Staining Kit	Thermo Fisher Scientific	Cat#LC6070
Proteomics Dynamic Range Standard Set	Sigma-Aldrich	Cat#UPS2
KOD hot-start polymerase	Merck Millipore	Cat#71086
Deposited Data		
MS raw and analyzed data	This paper	ProteomeXchange: PXD004185
Immunoblotting and PLA raw data	This paper	http://dx.doi.org/10.17632/jch2434thg.1
Experimental Models: Cell Lines		
HEK293T	Laboratory of Michiel Vermeulen	N/A
HeLa Cells	Spruijt et al., 2013	N/A
IB10 Cells	Spruijt et al., 2013	N/A
NPCs	Spruijt et al., 2013	N/A
HEK293T-EGFP-TAB-NZFs	This paper	N/A
Recombinant DNA		
pGEX-5X-1	GE healthcare Life Sciences	Product code: 28-9545-53
pGEX-4T-1	GE healthcare Life Sciences	Product code: 28-9545-49
GST-USP37-UIM1	This paper	N/A
GST-USP37-UIM2	This paper	N/A
GST-USP37-UIM3	This paper	N/A
GST-USP37-UIM12	This paper	N/A
GST-USP37-UIM23	This paper	N/A
GST-USP37-UIM123	This paper	N/A
GST-USP25-UBA	This paper	N/A
GST-USP25-UIM1	This paper	N/A
GST-USP25-UIM2	This paper	N/A
GST-USP25-UIM12	This paper	N/A

(*Continued on next page*)

Continued

REAGENT OR RESOURCE	SOURCE	IDENTIFIER
GST-USP25-UIM-N-term	This paper	N/A
GST-ANKRD13A-UIM12	This paper	N/A
GST-ANKRD13A-UIM23	This paper	N/A
GST-ANKRD13A-UIM34	This paper	N/A
GST-ANKRD13A-UIMs	This paper	N/A
GST-ANKRD13B-UIM12	This paper	N/A
GST-ANKRD13B-UIM23	This paper	N/A
GST-ANKRD13B-UIMs	This paper	N/A
GST-EPS15L1-UIMs	This paper	N/A
GST-DNAJB2-UIMs	This paper	N/A
GST-EPN3-UIMs	This paper	N/A
GST-PARP10-UIMs	This paper	N/A
GST-UCHL3	This paper	N/A
GST-TAB2-NZF	This paper	N/A
GST-TAB3-NZF	This paper	N/A
GST-TAB-NZFs	This paper	N/A
GFP-TAB-NZFs	This paper	N/A
GST-RAD23A-UBA2	This paper	N/A
pLV	Zhang et al., 2013a	N/A
pCR3.1	Zhang et al., 2013a	N/A
pMDLg-RRE (gag/pol)	Zhang et al., 2013a	N/A
pCMV-VSVG	Zhang et al., 2013a	N/A
pRSV-REV	Zhang et al., 2013a	N/A
Flag-His-UCHL3	This paper	N/A
RNF168-Myc	This paper	N/A
Flag-UCHL3	This paper	N/A
Flag-UCHL3-C95S	This paper	N/A
Flag-UCHL3-H169A	This paper	N/A
Flag-UCHL3-D184A	This paper	N/A
Flag-USP40	This paper	N/A
HA-K0-Ubiquitin	Lim et al., 2005	Addgene plasmids # 17603
His-HA-K6-Ubiquitin	This paper	N/A
His-HA-K11-Ubiquitin	This paper	N/A
His-HA-K27-Ubiquitin	This paper	N/A
His-HA-K29-Ubiquitin	This paper	N/A
His-HA-K33-Ubiquitin	This paper	N/A
His-HA-K48-Ubiquitin	This paper	N/A
His-HA-K63-Ubiquitin	This paper	N/A
Flag-K6-Ubiquitin	This paper	N/A
shUCHL3	This paper	N/A
Sequence-Based Reagents		
Streptavidin Sepharose	GE healthcare Life Sciences	Cat#17-5113-01
Ni-NTA Agarose	QIAGEN	Cat#30230
Glutathione Sepharose	Thermo Fisher Scientific	Cat#16101
glutathione Sepharose 4B beads	GE healthcare	Cat#17-0756-05
Flag resin	Sigma-Aldrich	Cat#A2220

(*Continued on next page*)

Continued

REAGENT OR RESOURCE	SOURCE	IDENTIFIER
GFP-Trap	Chromotek	N/A
Fmoc Gly TentaGel R Trt resin	RAPP POLYMERE GmbH	Cat#RA1213
Software and Algorithms		
MaxQuant	Cox and Mann, 2008	http://www.biochem.mpg.de/5111795/maxquant
Perseus	Cox and Mann, 2012	http://www.biochem.mpg.de/5111810/perseus
R		https://www.r-project.org
Other		
SMART database	Letunic et al., 2015	http://smart.embl-heidelberg.de

CONTACT FOR REAGENT AND RESOURCE SHARING

Further information and requests for resources and reagents should be directed to and will be fulfilled by the Lead Contact Michiel Vermeulen (michiel.vermeulen@science.ru.nl).

EXPERIMENTAL MODEL AND SUBJECT DETAILS

HEK293T cells, HeLa cells, mouse embryonic stem cells and neuronal progenitor cells were cultured as indicated in method details

METHOD DETAILS

Cell culture and extract preparation

HEK293T, HeLa cells were cultured in Dulbecco's Modified Eagle's Medium (DMEM, Thermo) supplemented with 10% Fetal bovine serum (FBS, Hyclone) and 1 × Penicillin/Streptomycin (15140-122, Thermo). For SILAC labeling, HeLa cells were cultured in SILAC DMEM (88420, Thermo) supplemented with 10% dialyzed FBS (DS-1003, Dundeecell), 1 × Glutamax (35050-061, Thermo), 1 × Penicillin/Streptomycin, 73mg/ml L-Lysine (light/K0, Sigma, A6969 or heavy/K8 Sigma, 608041) and 29.4mg/ml Arginine (light/R0 Sigma, A6969 or heavy/R10 Sigma, 608033). Mouse embryonic stem cells (ESCs) IB10 were cultured in DMEM supplemented with 15% FBS, 1 × Glutamax, 1 × Penicillin/Streptomycin, 1 × Non-essential amino acids (11140-035, Thermo), 1 × sodium pyruvate (11360-070, Thermo), LIF (1000 U/ml), 0.1 mM β-mercaptoethanol (M6250, Sigma). Neuronal progenitor cells (NPCs) derived from IB10 cells were cultured on gelatin coated dishes in medium containing of NSA MEM (Euromed EVM0883LD), 1 × Glutamax, 1 × N2 supplement (17502-048, Thermo), 10 ng/ml bFGF (RD systems 233-F3) and 10 ng/ml EGF (235-E9) (Spruijt et al., 2013). ESCs and NPCs were detached from culture plates using accutase (A11105-01, Thermo). Antibodies used for ESC and NPC markers are: Oct-4 (sc-5279, Santa Cruz), Nanog (14-5761-80, Affymetrix) and Nestin (556309, BD).

Whole cell extracts were prepared by adding 5 cell pellet volumes of lysis buffer (0.5% NP40, 150 mM NaCl, 50 mM Tris pH 8.0, 10% Glycerol and 1 × Complete Protease Inhibitors). Cells were vortexed for 30 s and then incubated for 2 hr on a rotation wheel. Samples were then centrifuged at 4700 rpm with a swinging bucket rotor for 30 min, after which soluble whole extracts were aliquoted and snap frozen until usage. Nuclear extracts were prepared essentially as described (Spruijt et al., 2013). Briefly, HeLa cells treated with DMSO or 1 μM doxorubicin (D1515, Sigma) for 6 hr were trypsinized and washed 2 times with PBS. Cells were then incubated for 10 min in 5 cell pellet volumes of Buffer A (10 mM HEPES KOH pH 7.9, 15 mM MgCl2, 10 mM KCl). After centrifugation at 400 g for 5 min, cells were lysed by dounce homogenization in 2 cell pellet volumes of Buffer A in the presence of 0.15% NP40 and 1 × complete protease inhibitors. After centrifugation at 3200 g with a swinging bucket rotor for 15 min, crude nuclei were lysed in 2 pellet volumes of nuclear extraction buffer (300 mM NaCl, 20 mM HEPES pH 7.9, 20% glycerol, 2 mM MgCl2, 0.2 mM EDTA, 0.1% NP40, 1 × complete protease inhibitor and 0.5 mM DTT) and incubation for 90 min in a rotation wheel. After centrifugation at 20000 g for 30 min, the soluble nuclear extract was aliquoted and snap frozen until further usage. All incubation steps were performed either on ice or at 4°C. The protein concentration of the lysates was measured using the BCA assay (23225, Thermo).

SILAC-based ubiquitin pull-down

For SILAC-based ubiquitin pull-downs, 25 μg His-tagged ubiquitin or linear hexa-ubiquitin chains (J2520, UBPbio) were immobilized on Ni-NTA agarose beads (30230, QIAGEN) in a total volume of 500 μL of peptide binding buffer (150 mM NaCl, 50 mM Tris pH 8.0, 0.1% NP40) and incubated for 1 hr in a rotation wheel at RT. For the forward experiment, beads coupled with ubiquitin or linear polyubiquitin chains were incubated with 5 mg of light and heavy whole cell extracts, respectively, in a total volume of 1 mL of protein lysis buffer containing 15 mM imidazole (I5513, Sigma). After incubation, beads from both pull-downs were combined after 4 washes with 1 mL of lysis buffer containing 1% NP40 and 20 mM imidazole. The reverse experiment constitutes a SILAC label swap control experiment.

In-gel and on-bead digestion

For in-gel digestion, beads were incubated in 40 μL of 2 × SDS loading buffer for 5 min at 95°C. Proteins were separated on 4%–20% gradient gels (4561094, BIO-RAD) and stained with Coomassie brilliant blue G-250 (161-0436, BIO-RAD). In-gel digestion was performed as described (Spruijt et al., 2013). Briefly, each gel lane was cut into 8 bands which were then cut into smaller (~1 mm) fragments. Gel pieces were destained in a thermoshaker at 1200 rpm at RT in 1 mL destain buffer (50% ethanol, 25 mM ammonium bicarbonate (ABC, 09830, Sigma)). Gel pieces were incubated in 10 mM DTT in 50 mM ABC for 45 min at 55°C and subsequently incubated in 55 mM iodoacetamide (IAA, I1149, Sigma) in 50 mM ABC for 10 min in a thermoshaker (1200 rpm) at RT in the dark. Proteins were digested overnight at 37°C with 300 ng of trypsin (V5280, Promega) in 50 mM ABC. Peptides were extracted from the gel in 30% acetonitrile/3% trifluoroacetic acid (TFA) and desalted using C18 (Empore) Stagetips prior to MS analyses.

Proteins were on-bead digested with trypsin as described before (Spruijt et al., 2013). In short, beads were resuspended in 100 μL of elution buffer (2 M urea, 10 mM DTT and 50 mM Tris pH 8.5) and then incubated for 20 min at RT in a thermoshaker at 1200 rpm. IAA was then added to a final concentration of 55 mM followed by a 10 min incubation in a thermoshaker (1200 rpm) at RT in the dark. Proteins were then partially digested from the beads by adding 250 ng of trypsin for 2 hr at RT in a thermoshaker in the dark. After incubation, the supernatant was collected in a separate tube. The beads were then incubated with 100 μL of elution buffer for 5 min at RT in a thermoshaker (1200 rpm). 200 ng of fresh trypsin was added to the pooled eluates and proteins were digested overnight at RT. Finally, tryptic peptides were acidified to pH < 2 by adding TFA and desalted using C18 Stagetips prior to MS analyses.

Synthesis of non-hydrolyzable diubiquitin

Preparation of ubiquitin precursors: To prepare distal ubiquitin precursor, ubiquitin$_{1-75}$ was synthesized as described earlier (El Oualid et al., 2010) via linear FMOC-based solid phase peptide synthesis (SPPS), using preloaded trityl resin (Fmoc Gly TentaGel R TRT resin, RA1213, Rapp polymere GmbH). The ethylene glycol spacer (8-(Fmoc amino)-3,6-dioxaoctanoic acid, 166108-71-0, AK scientific) was coupled on resin to the N terminus of the polypeptide in the final steps of solid phase peptide synthesis. The resin was next swollen by washing with N-Methyl-2-pyrrolidone (NMP), and biotin (B4501, Sigma) was coupled to 25 μmol peptide in 1 mL reaction mixture (4 eq. biotin dissolved in NMP; 4 eq. HOBT and 4 eq. HBTU dissolved in DMF; 8 eq. DIPEA dissolved in NMP) for 3 hr. The protected polypeptide was released from the resin using a mild hexafluoroisopropanol (HFIP)/dichloromethane (DCM) (1:4, v/v) cleavage for 30 min that leaves the globally protected polypeptide intact. After evaporation of the solvent, the solid was co-evaporated 3 times with dichloroethane (DCE) to remove HFIP traces. The peptide (25 μmol) was dissolved in DCM (1 ml/5 μmol) and reacted with 5 eq. PyBOP, 5 eq. triethylamine and 10 eq. propargylamine (PA) for 16 hr. The reaction mixture was concentrated and excess PA was removed by co-evaporation with DCM and toluene. Protected biotin-PEG-Ub$_{1-75}$ PA was dissolved in DCM and extracted with 1 M $KHSO_4$ and sat. aq. NaCl before drying the organic layer using sodium sulfate and concentration. Final deprotection was achieved by TFA cleavage (90.5% TFA, 5% TIS, 2.5% H_2O, 2% phenol) for 2.5 hr.

For proximal ubiquitin (Ub azido ornithine and Ub α-azido norleucine), Ubiquitin$_{1-76}$ was synthesized as described earlier (El Oualid et al., 2010) and azide containing amino acids were incorporated at the desired positions during SPPS. To avoid oxidation, methionine 1 was replaced by the close analog norleucine. α-azido norleucine was prepared as described earlier (Moss et al., 2012) and incorporated during solid phase peptide synthesis. FMOC protected azido ornithine was purchased from Sigma (714291).

To purify ubiquitin precursors, crude products were dissolved in 5% warm DMSO and further diluted in Milli-Q water. NaOAc buffer was added to a final concentration of 50 mM NaOAc pH 4.5 and the precursors were applied to a 40 mL 40S Workbeads (Bio-Works) cation column. The product was eluted over a gradient of 0-1 M NaCl in 10 column volumes at a flow of 12 ml/min and further purified by a C18 RP-HPLC column (Atlantis prep T3, 10x150 mm, 5 μm particle size) using a linear gradient between 20%–70% B in 12 min (A = 95/5/0.05% H_2O/ACN/TFA, B = 5/95/0.05% H2O/ACN/TFA). Fractions were analyzed by LC-MS (LCTTM Orthogonal Acceleration Time of Flight Mass spectrometer, Micromass) and lyophilized in freeze dry mix (65% H2O, 25% ACN, 10% acetic acid).

Synthesis of diubiquitin: Biotin-Ub-PA (1 eq.) and Ub-N3 (1.5 eq) precursors were dissolved in hot DMSO (2.5% v/v) and diluted in 8M urea/100 mM phosphate pH 7 buffer to a total concentration of 4 mg/ml. CuSO4 (100 mM in Milli-Q water; C8027, Sigma), sodium ascorbate (600 mM in Milli-Q water; PHR1279, Sigma) and TBTA ester (100 mM in ACN) (Zhou and Fahrni, 2004) were pre-mixed in equal volumes and added to a final concentration of 1.25 mM, 7.5 mM and 1.25 mM respectively. All solutions were degassed by bubbling with argon for approximately 5 min before dissolving the reagents. Click reactions were followed by LC-MS (LCTTM Orthogonal Acceleration Time of Flight Mass spectrometer, Micromass) and afterward purified by a C18 RP-HPLC column as described above. Fractions containing the correct product were lyophilized in freeze drying mix (65% H_2O, 25% ACN, 10% acetic acid) and afterward dissolved in 5% hot DMSO, 20 mM Tris pH 7.6 and 150 mM NaCl. Further separation of monoubiquitin from diubiquitin was achieved through size exclusion using a HiLoad 16/600 Superdex75 pg column (GE healthcare) and fractions were analyzed by SDS-PAGE. All non-hydrolyzable diubiquitins were further verified by analytical LC-MS.

Label free pull-down

For label free pull-downs, 25 μg of each diubiquitin was incubated with 25 μL of streptavidin Sepharose beads (17-5113-01, GE life Sciences) in 500 μL of peptide binding buffer for 1 hr at RT in a rotation wheel. Beads containing immobilized diubiquitins were then incubated with 5 mg of whole cell or 3 mg of nuclear extracts in a total volume of 1 mL of lysis buffer (NP40 was added to a final concentration of 0.5% for nuclear extracts) on a rotation wheel at 4°C. Beads were then washed 4 times with 1 mL of lysis buffer containing 1% NP40 and 2 times with 1 mL of PBS. Each experiment was performed in triplicate and bound proteins were subjected

to on-bead digestion as described above. For different length linear ubiquitin chain pull-downs, 25 μg His-tagged ubiquitin (E1301, UBPbio), linear tetra-ubiquitin ((D4430, UBPbio)) and linear hexa-ubiquitin chain (D4410, UBPbio) were used.

For immunoblotting-based diubiquitin pull-downs, input protein amounts were scaled down by a factor of 3. Used antibodies for western blotting: MBD3 (sc-9402, Santa Cruz), ACTL8 (17312-1-AP, Proteintech), HDAC6 (12834-1-AP, Proteintech), IKBKG (sc-8330, Santa Cruz), MYCBP (12022-1-AP, Proteintech), BRE (11702-1-AP, Proteintech), RAD23A (11364-1-AP, Proteintech), ATXN3 (13505-1-AP, Proteintech), UCHL3 (12384-1-AP, Proteintech), EPS15R/EPS15L1 (21243-1-AP, Proteintech), USP19 (25768-1-AP, Proteintech), ADRM1 (11468-1-AP, Proteintech), TAB2 (14410-1-AP, Proteintech) and USP25 (12199-1-AP, Proteintech).

Recombinant protein purification

To purify His-Flag tagged UCHL3 from cells, UCHL3 amplified from HeLa cDNA was cloned into a lentivirus vector with N-terminal 6 × His and Flag tags. Lentiviruses were produced by transfecting the indicated plasmids together with helper plasmids pCMV-VSVG, pMDLg-RRE (gag/pol), and pRSV-REV into HEK293T cells as described before (Zhang et al., 2013a). Cell supernatants were harvested at 48 hr post transfection. To obtain stable cell lines, HEK293T cells were infected for 24 hr with lentivirus supernatant in the presence of 5 μg/ml of polybrene (107689, Sigma). After infection, cells were re-seeded into p15 plates with 1 μg/ml puromycin (P7130, Sigma) for 3 days. HEK293T cells stably expressing Flag-His-UCHL3 protein lysed with TNE lysis buffer (100 mM Tris pH7.5, 150 mM NaCl, 0.5 mM EDTA and 1% NP40) were immunoprecipitated with nickel agarose overnight at 4°C, followed by 5 elutions with TNE lysis buffer with 300 mM imidazole. Pooled eluates were subsequently immunoprecipitated with Flag resin (A2220, Sigma), followed by 5 elutions with 150 mg/ml 3 × Flag peptide (A6001, APExBIO) in PBS. Flag peptides were discarded and eluates were concentrated using Amicon Ultra 3K (Millipore).

To express recombinant proteins, indicated deletions of each gene were cloned into pGEX-5X-1 vector (for the UBA2 domain of RAD23A, pGEX-4T-1 vector, courtesy of Dr. Koraljka Husnjak, was used). Four tandem repeats of the TAB2 NZF domain with a flexible linker region (GlyGlyGlySerGlyGlyGly) synthesized by Integrated DNA Technologies were also cloned into pGEX-5X-1 vector. Protein expression was performed in BL21 *E.Coli*. Bacteria were grown at 37°C until OD600 0.8, after which protein expression was induced overnight at 16°C by adding 0.5 mM IPTG (V3951, Promega). Cells were lysed in 50 mM Tris-HCl pH 7.5, 100 mM NaCl, 10% glycerol, 0.5 mM EDTA, 0.5 mM PMSF, 1 mM DTT, 0.05% NP40, 1 × complete protease inhibitor and 0.5 mg/ml lysozyme with repeated freeze-thawing. 0.5% NP40, 5 mM MgCl2 and 25 μg/μl DNase I (04716728001, Sigma) were sequentially added to the lysates followed by an additional incubation for 30 min at 4°C to digest DNA. The remaining suspension was centrifuged at 20000 g for 30 min, after which the soluble extract was aliquoted and snap frozen until further usage. For Biolayer Interferometry (BLI) assay, glutathione Sepharose 4B beads (GE healthcare; 17-0756-05) bound TAB2 NZF domain and RAD23 UBA2 proteins were washed with washing buffer (20 mM Tris pH 7.6, 150 mM NaCl, 2 mM DTT) 3 times, and eluted with 20 mM reduced glutathione (00159, Chem-IMPEX). The GST tag was removed during overnight cleavage using Factor Xa (P8010, NEB) for TAB2 NZF and Thrombin (27-0846-01, GE healthcare) for RAD23A UBA2 domain. Pure ubiquitin binding domains were obtained through a final a size exclusion step in 20 mM Tris pH 7.5, 150 mM NaCl, 2 mM DTT (Superdex 75 16/600; 28989333, GE healthcare).

In vitro interaction assay

500 ng of biotin tagged ubiquitin or diubiquitins were incubated with GST tagged proteins (10 μg) immobilized on glutathione Sepharose (16101, Thermo) in a lysis buffer containing 0.5% NP40, 150 mM NaCl, 50 mM Tris pH 8.0, 10% glycerol and 1xcomplete Protease Inhibitors. Beads were then washed 4 times with lysis buffer containing 1% NP40 and analyzed by SDS-PAGE. The interactions between biotin-tagged diubiquitin and GST fusion protein were visualizing by immunoblotting using an HRP-streptavidin antibody (PA1-26848, Thermo) on PVDF membranes denatured by guanidinium chloride buffer (6 M GnHCl, 20 mM Tris pH7.5, 5 mM β-mercaptoethanol, 1 mM PMSF) for 30 min at 4°C. For in vitro interaction studies between the TAB2/3 NZF domain and native diubiquitin (J2000, UBPBio), a silver staining kit (LC6070, Thermo) was used to detect the interaction after the pull-downs. In vitro interaction assays between UCHL3 and non-hydrolyzable diubiquitin were performed with biotin tagged diubiquitins (5 μg) immobilized on streptavidin beads and incubation with UCHL3 protein. UCHL3 protein was produced as described previously (Larsen et al., 1996). Western blotting was in this case performed with a UCHL3 antibody. For interaction studies between UCHL3 and native diubiquitin (homemade, see below), 5 μg of GST-UCHL3 coupled to glutathione Sepharose was incubated with 2 μg of monoUb or native diubiquitins. Coomassie brilliant blue G-250 was then used to stain the proteins after the pull-downs.

Affinity and kinetic measurements with BLI

Native diubiquitins were obtained using native chemical ligation as described previously (El Oualid et al., 2010) and Met-1 diubiquitin was obtained from expression in *E. coli* BL21 cells. Lysine-linked diubiquitins were purified as described above for the non-hydrolyzable diubiquitins through HPLC and size exclusion and Met1-linked diubiquitin was purified as described by Larsen et al., 1996. Native diubiquitins were then biotinylated on a random primary amine site with EZ-linkTM NHS-LC-LC-biotin (21343, Thermo) in 25 mM HEPES, pH 7.6 and 150 mM NaCl. Labeling was performed in a 1:2 biotin to diubiquitin ratio to avoid double biotinylation of diubiquitins. After overnight labeling at 4°C, the extent of biotinylation was monitored by LC-MS. In general, all diubiquitins showed 50%–60% mono biotinylation and 10%–15% double biotinylation, while the remaining fraction was not biotinylated. All biotinylated native diubiquitins were further purified using a Superdex 75 10/300 size exclusion column (17-5174-01, GE healthcare) to separate diubiquitins from unreacted biotin.

Affinity and kinetic measurements were performed using BLI on an Octet Red96 instrument (FortéBio) using streptavidin coated biosensors (part. no. 18-5019, FortéBio) and immobilization of N-terminally biotinylated non-hydrolyzable diubiquitins or randomly biotinylated native diubiquitins (ligand). All measurements were performed using standard kinetic settings (5.0 Hz, averaging by 20) at 30°C. Ligand density scouting was monitored for N-terminally biotinylated non-hydrolyzable K27 diubiquitin at 25, 50, 100, 200 or 400 nM diubiquitin and found optimal at a concentration of 50 nM diubiquitin during a loading step of 180 s. Similarly, the optimal ligand density for randomly biotinylated native diubiquitins (25, 50, 100, 200 and 400 nM) was determined at 200 nM immobilization for 180 s.

UCHL3 BLI binding experiments were performed in binding buffer (50 mM Tris pH 7.6, 150 mM NaCl, 0.5 mM EDTA, 5 mM DTT, 0.005% Tween-20) using a baseline step of 60 s, an association phase of 60 s and a dissociation phase of 180 s.

Enrichment of cellular ubiquitin linkages by the TAB NZF domain

Four tandem repeats of TAB NZF domains were cloned into a lentivirus vector with an N-terminal EGFP tag. HEK293T cells stably expressing EGFP-TAB-NZFs or transient expressing His-Myc-ubiquitin were constructed by lentiviral infection or transfection as described above. GFP-Trap beads (Chromotek) were used to affinity enrich the EGFP-TAB-NZFs protein and interacting proteins from whole cell lysates. His-Myc-tagged ubiquitin was also enriched from whole cell lysates using nickel beads. Affinity enriched proteins with on-bead digested with trypsin as described above except that CAA (2-Chloroacetamide; C0267, Sigma) instead of IAA was used for peptide alkylation. In addition, the protein sequence of the His-Myc-ubiquitin plasmid was included into the uniprot database that was used to search the mass spectrometry data. Furthermore, the glycine-glycine ubiquitin remnant was added as a variable modification during the MaxQuant database searches.

In vitro and in vivo deubiquitination assay

For in vitro deubiquitination assay, 500 ng of recombinant UCHL3 or His-Flag tagged UCHL3 purified from HEK293T cells was incubated with 200 ng of diubiquitins (J2000, UBPBio) in a total volume of 30 μL cleavage buffer (50 mM Tris pH 7.5, 50 mM NaCl and 5 mM DTT) at 37°C. 10 μL aliquotes of the reactions were mixed with 5 μL of 4 × LDS loading buffer (NP0007, Thermo) at the indicated time points to stop the reaction. Samples were then subjected to SDS-PAGE in MES running buffer (50 mM MES, 1% SDS, 1 mM EDTA and 50 mM Tris) and proteins were visualized by silver staining.

For in vivo deubiquitination assay, UCHL3 and RNF168 were amplified from HeLa cDNA using KOD hot-start polymerase (71086, Millipore) and cloned into pCR3.1 vector with a N-terminal Flag tag and into pLV vector with a C-terminal Myc tag, respectively. Point mutations of UCHL3 were also introduced using KOD hot-start polymerase. HA-K0 ubiquitin from Ted Dawson (Addgene plasmids # 17603) was used as a template to clone 6 × His and HA tagged K-only ubiquitin mutants (Lim et al., 2005). Sequence "GTCTTACTTCTCTTTCCTAT" which targets human UCHL3 was cloned into an inducible shRNA knock-down construct as described before (Herold et al., 2008). HEK293T cells stably expressing UCHL3 shRNA were prepared using lentivirus as described above. In vivo deubiquitination analyses by Ni-NTA pull-downs were performed as described before (Zhang et al., 2013b). In short, cells transfected with the indicated plasmids were washed 2 times in cold PBS with 10 mM NEM (E3876, Sigma) and lysed in 2 mL 8 M urea buffer (8 M urea, 0.1 M Na_2HPO4, 0.1 M NaH_2PO4, 10 mM Tris-HCl, 10 mM imidazole, 10 mM β-mercaptoethanol). Lysates were centrifuged at 16000 g for 10 min and incubated with nickel beads for 2 hr at RT. Beads were then washed 4 times with 8 M urea buffer containing 20 mM imidazole, and incubated with 30 μL of 2 × SDS buffer at 37°C for 20 min before analysis with SDS-PAGE. Antibodies used for western blotting: Flag (F3165, Sigma), Myc-tag (sc-789, Santa Cruz), HA-tag (sc-805, Santa Cruz), ACTIN (A5441, Sigma) and GFP (ab290, Abcam and sc-8334, Santa Cruz).

Proximity ligation assay (PLA)

HeLa cells grown on Lab-Tek II 8 wells chamber slides (154534, Thermo) were transfected with empty vector or Flag-tagged K6-only ubiquitin plasmid. 36 hr after transfection cells were stimulated with DMSO or 1 μM doxorubicin for 6 hr. Cells were washed twice with PBS, and fixed with 3% Formaldehyde (104003, Merck Millipore) for 30 min at RT. Subsequently, cells were quenched with 2 mg/ml glycine in PBS, permeabilized with 0.2% Triton X-100 in PBS, and washed 3 times with PBS. The proximity ligation assay (PLA) were performed according to the manufacturer's protocol (DUO92101, Sigma). Used antibodies: Flag (1:200 dilution, F3165, Sigma), CDKN2A (1:100 dilution, A301-267A-T, Bethy) and CDK7 (1:100 dilution, A300-405A-T, Bethy). Images were visualized using a confocal microscope (Olympus FV1000 + TIRF).

Global absolute protein quantification

iBAQ was performed as described before (Spruijt et al., 2013). 3.3 μg of UPS2 standard (Sigma) was added to lysates from 4×10^4 IB10 cells or 6×10^4 NPCs (≈ 10 μg WCE in 8M urea buffer containing 0.1 M Tris pH 8.5), which was digested using the FASP protocol (filter aided sample preparation method) (Wiśniewski et al., 2009). In brief, proteins were added onto 30 kDa cut-off filter and centrifuged at 11000 rpm at 20°C for 15 min. 50 mM IAA in urea buffer was used to alkylate proteins at 20°C for 15 min. After few washes with urea and 50 mM ABC buffer, 100 ng of trypsin in 50 mM ABC buffer was used to digest proteins in a wet chamber overnight at 37°C. Peptides was extracted by 50 mM ABC buffer and acidified by TFA. In addition, 100 μg of ESC or NPC WCE was digested using an additional SAX protocol. After the FASP protocol as described above, the peptides were separated into 5 fractions (flow through, pH 11, pH 8, pH 5, pH 2). Each of these samples was measured in a 4 hr gradient of LC-MS/MS.

Mass spectrometry analysis

Tryptic peptides were separated with an Easy-nLC 1000 connected online to mass spectrometer (Thermo). In-gel digestion samples were separated using a 94 min gradient of acetonitrile (7% to 32%) following by washes at 50% then 95% acetonitrile for 120 min of total data collection. Top 10 most abundant peptides were fragmented for ms/ms and mass spectra were recorded on a LTQ-Orbitrap QExactive mass spectrometer (Thermo). Peptides from on-bead linear hexa-ubiquitin pull-downs and endogenous ubiquitin linkages identification by GFP-TAB2 NZF domains were separated using a 114 min gradient of acetonitrile (7% to 32%) following by washes at 50% then 95% acetonitrile for 140 min of total data collection. Scans were collect in data-dependent top-speed mode with dynamic exclusion set at 60 s. Mass spectra were recorded on a LTQ-Orbitrap Fusion Tribrid mass spectrometer (Thermo). Peptides from remaining experiments were separated using a 214 min gradient of acetonitrile (7% to 30%) following by washes at 60% then 95% acetonitrile for 240 min of total data collection.

QUANTIFICATION AND STATISTICAL ANALYSIS

BLI data analysis

All BLI measurements were referenced against an empty biosensor which also served to monitor non-specific binding of the analyte to the biosensor surface. Kinetic analysis was determined using a global fit with the Association Kinetics (two ligand concentrations) model in GraphPad Prism 7. Steady state analysis was determined by averaging the response of the association phase after the steady state was reached for UCHL3 and by averaging the complete association phase (30 s) for the ubiquitin binding domain experiments. Obtained steady state data was fitted using nonlinear regression least-squares fit and using One Site-Total model (GraphPad Prism 7), with the exception of the RAD23A UBA2 domain. In this case, UBA2 binding to native K48 and K63 was fitted using nonlinear regression robust fit.

Mass spectrometry data analysis

For SILAC-labeling based experiments, raw data were analyzed using MaxQuant version 1.5.0.1 with default settings and Arg10/Lys8 heavy or light labels, and match between runs enabled (Cox and Mann, 2008). Normalized ratios were plotted for the forward and reverse pull-downs. Outliers were identified independently in the forward and reverse pull-downs using boxplot statistics (threshold: 1.5 x the interquartile range (IQR)). Proteins were considered significant if they were identified as outliers in both experiments.

For label-free pull-downs, raw data were analyzed using MaxQuant version 1.5.0.1 with default settings and match between runs and label-free quantification (LFQ) enabled. Identified proteins were filtered for reverse hits and common contaminants. Additionally, proteins were filtered to be detected in all replicates of at least one triplicate experiment. LFQ intensities were log2 transformed and missing values were semi-random imputed from a normal distribution (width = 0.3 and shift = 1.8) in Perseus (Cox and Mann, 2012), based on the assumption that these proteins were just below the detection limit. Enrichments were normalized by row mean subtraction, before significantly enriched proteins were identified by an ANOVA test (thresholds indicated in the text for the specific experiments). Enriched proteins were clustered on correlation (complete linkages) and plotted as heatmaps or spider plots in R. Additionally, K-means clustering was done in R as well as plotting of scatterplots, Venn diagrams and boxplots. Gene ontology annotation was added using Perseus and enriched terms were identified by a Fisher's exact test comparing significant interactors and background proteins. DUBs were manually selected. Protein domains were annotated using the SMART database and manually curated (Letunic et al., 2015).

For absolute quantification of ESC and NPC proteomes, raw data were analyzed using MaxQuant version 1.5.0.1, with iBAQ enabled. Identified proteins were filtered for reverse hits and common contaminants. Mass spectrometry analyses were performed of the lysates containing UPS2 standard and resulted in the quantification of ~4000 proteins using linear regression between the iBAQ intensity (log10 transformed) and known amounts (log10 transformed) of the UPS2 standard proteins and the absolute amounts of all proteins were extrapolated (Figure S3C "UPS2" plots). To increase proteome depth, strong-anion-exchange (SAX) fractionation of the cellular lysate was performed. To absolutely quantify all proteins in these deep proteomes, linear regression was performed between the absolute amounts of the ~4000 initially quantified proteins (log10 transformed) and their measured iBAQ intensity (log10 transformed) in the fractionated samples (Figure S3C "FASP vs SAX" plots) to extrapolate the absolute amounts of all proteins identified in the SAX proteome.

DATA AND SOFTWARE AVAILABILITY

Software

MaxQuant and Perseus were used to process raw mass spectrometry data, and R was used to make the graphs (Cox and Mann, 2008, 2012).

Data Resources

The accession number for the mass spectrometry data reported in this paper is ProteomeXchange: PXD004185 (Vizcaíno et al., 2016). The unprocessed image files used to prepare the figures in this manuscript have been deposited to Mendeley Data and are available at http://dx.doi.org/10.17632/jch2434thg.1.